POLITECNICO DI TORINO
Repository ISTITUZIONALE

Control of a Noncooperative Approach Maneuver Based on Debris Dynamics Feedback

Original
Control of a Noncooperative Approach Maneuver Based on Debris Dynamics Feedback / Corpino, Sabrina; Mauro, Stefano; Pastorelli, Stefano; Stesina, Fabrizio; Biondi, Gabriele; Franchi, Loris; Mohtar, Tharek. - In: JOURNAL OF GUIDANCE CONTROL AND DYNAMICS. - ISSN 0731-5090. - STAMPA. - 41:2(2018), pp. 431-448. [10.2514/1.G002685]

Availability:
This version is available at: 11583/2689334 since: 2018-03-07T10:28:27Z

Publisher:
American Institute of Aeronautics & Astronautics

Published
DOI:10.2514/1.G002685

Terms of use:

This article is made available under terms and conditions as specified in the corresponding bibliographic description in the repository

Publisher copyright

(Article begins on next page)

28 March 2024

Control of a non-cooperative approach maneuver based on debris dynamics feedback

Sabrina Corpino[1], Stefano Mauro[2], Stefano Pastorelli[3], Fabrizio Stesina[4], Gabriele Biondi[5], Loris Franchi[6], Tharek Mohtar[7]
Politecnico di Torino, Torino, Italy, 10129

Space Debris removal is a critical issue related to space research. One of the key requirements for a removal mission is the assessment of the target rotational dynamics. Ground observations are not sufficient for reaching the accuracy level required to guide the chaser spacecraft during the capture maneuver. Moreover, the guidance and control strategy for the chaser to approach the target is a critical aspect of such missions. This paper present simulation results of two complementary methods, one for estimating the entire rotational dynamic state of the target, and the other for accurately controlling the approach maneuver. In particular, the information coming from the identification and prediction of the actual motion of the rotation axis of the target is exploited by the second method for aligning the docking interface of the chaser with that axis at the instant of capture. The dynamic estimation is based on Kalman filtering in an original combination with compressive sampling techniques for making the method robust to failures of the observation sensors. The guidance of the chaser is based on a model predictive control law. The combined simulation of the employment of the methods has revealed the feasibility of the global approach.

I. .Introduction

ONE of the main concerns in the space field is the high number of objects orbiting the Earth in orbits of interest for the accomplishment of scientific and communication missions. Currently, more than 10000 objects bigger than 10 cm take up Low Earth Orbit (LEO) and Geosynchronous Earth Orbit (GEO) [1].

In recent years, the international community decided to adopt rules specifically aimed at the Post Mission Disposal (PMD). These guidelines require that any orbiting element shall be removed from the operative orbit within 25 years

[1] Assistant Professor, Department of Mechanical and AeroSpace Engineering, Corso Duca degli Abruzzi 24, Torino
[2] Assistant Professor, Department of Mechanical and AeroSpace Engineering, Corso Duca degli Abruzzi 24, Torino
[3] Associate Professor, Department of Mechanical and AeroSpace Engineering, Corso Duca degli Abruzzi 24, Torino
[4] Post-Doc Researcher, Department of Mechanical and AeroSpace Engineering, Corso Duca degli Abruzzi 24, Torino
[5] PhD Candidate, Department of Mechanical and AeroSpace Engineering, Corso Duca degli Abruzzi 24, Torino
[6] PhD Candidate, Department of Mechanical and AeroSpace Engineering, Corso Duca degli Abruzzi 24, Torino
[7] PhD Candidate, Department of Mechanical and AeroSpace Engineering, Corso Duca degli Abruzzi 24, Torino

following the end of its service life. However, even if all new spacecraft will comply with the PMD rules, this is not sufficient to reduce the risk of overpopulated orbits [2], considering the spacecraft already launched in the previous years. The LEGEND model [3] shows how a plan of Active Debris Removal (ADR) of non-collaborative spacecraft is strongly required. The general approach for removing space debris consists in the capture of a non-collaborative Target using a Chaser spacecraft. Capturing an object in orbit is a complex task, which requires many maneuvers to be accomplished, depending on the specific mission. Two of the main issues, common to most debris removal missions, is to understand the Target motion that is unknown a priori into the detail, and to plan a set of Chaser's maneuvers to complete the capture.

The capture of space debris is a deeply theorized problem but there are few examples of programs targeted to Rendez-Vous and Docking (RVD) missions for active debris removal and they mainly address the technology for the capture. One example is the Automated/Autonomous Rendezvous & Docking Vehicle (ARDV), which aims at testing in orbit a high performance laser sensors [4]. The CleanSpace One program of the Ecole Polytechnique Federale de Lausenne proposes a solution to perform active debris removal with a cost effective microsatellite. The approach and in-orbit maneuvering will be performed by a micro-propulsion system and the grabbing will be done by means of a robotic claw [5]. Similarly, the Remove DEBRIS mission aims at demonstrating key ADR technologies, including capture means (net and harpoon firing on a distant Target), relative navigation techniques (vision-based navigation sensors and associated algorithms), and deorbiting technologies (drag sail deployment after the mission followed by an uncontrolled reentry) [6]. Astrium Stevenage is developing a new technology (scheduled for launch in 2021) based on a harpoon system as debris capture mechanism. [7]

Other researches, independent from planned missions or official space programs, are ongoing. Sommer and Ahrns [8] propose solutions both for the trajectory and the attitude determination and control of a chaser involved in the removal of the Envisat satellite. Wertz and Bell [9] give an overview of hardware and software technologies (sensors and actuators) required for the autonomous rendezvous and docking of two spacecraft started at a remote distance. Cresto Aleina et alii [10] show the system design for a space tug involved in satellite servicing mission, such as the removal of out of order satellites.

From the maneuvers strategies point of view, Di Cairano et alii [11] give a complete overview of the maneuver and control capabilities for the capture of a non-rotating and of a rotating target, using a Model Predictive Controller (MPC) but limiting the study to planar maneuvers. In [12], the authors study controllers based on Linear Quadratic

Regulator (LQR) and Proportional Derivative (PD) Control, verifying the performance and robustness of the solutions. Similarly, Arantes et alii [13] use the same control laws and presents a comparative analysis between different guidance trajectories for important parameters such as time, fuel consumption minimum absolute distance and the maximum radial distance from the target. Adaptive control laws for spacecraft rendezvous and docking under measurement uncertainty, such as aggregation of sensor calibration parameters, systematic bias, or some stochastic disturbances, are proposed in [13],[14]. Aghili [15], and Matsumoto et alii [16] propose control laws solutions for the capture of tumbling target using a robotic arm. Authors study how to search an optimal mating point and trajectory, and demonstrate with simulations that robots intercept the point of grapple with quasi zero velocity and a high accuracy also when the target's dynamics is not known a priori and with the presence of uncertainties.

In the present paper, authors present guidance strategies based on Model Prediction Controllers, designed taken into account internal and external disturbances and uncertainties on the parameters. The Controller allows to perform a series of complex maneuvers that consist of reaching a point on a generic capture axis through a fly-around maneuver and then completing the capture along that axis with a straight line maneuver.

In order to define the best guidance strategy, one of the essential points is the availability of the accurate estimation of the kinematic and dynamic behavior of the tumbling uncooperative object. The estimation of the unknown dynamic state of space debris is a delicate issue because no direct information about the attitude of the object is available and then it must be obtained exploiting external sensors on the chaser. Some important results were obtained in the recent past through the usage of 3D active sensors: one example is given in [17], where the geometry and the attitude of space debris are determined from range images. Also in [18] a method for the pose estimation of passive space bodies based on a laser 3D scanner is presented. This last method covers the possibility of failures during the scanning procedure through efficient estimation algorithms but it requires the availability of a CAD model of the object. Solutions with passive sensors could be interesting because allow to save energy. Moreover, the exploitation of passive sensors permits of recovering the attitude and then the dynamic state of the Target by knowing the location of some features on its external surface. A survey of the most common tracking techniques based on stereovision can be found in [19]. In [20] and [21] two different methods are presented to maintain, after the rendezvous phase, a Target space body into the field of view (FOV) of the cameras on a Chaser spacecraft.

On the contrary, the main drawback of the techniques based on passive sensors derives from the presence of different phenomena, such as occlusions or disturbing reflections that make discontinuous and inaccurate the tracking of the

natural features of space objects. In spite of this, several authors have recently made some effort in the attempt to prove the effectiveness of these systems. In [22], a 3D model matching technique is used in combination with stereovision sensors. The considered method requires a high number of detected features and a very detailed model of the failed satellite. Segal S., Carmi A.,and Gurfil P. [23] presented a method based on stereovision to track a non-cooperative spacecraft estimating its complete dynamic state. The method does not require any a-priori information about the Target, but it is supposed that the position of several fixed features is always measurable. Thus, if at least three features are not temporarily detectable due to occlusions, the method loses its estimation capabilities. In [24], the tracking of a Target body with respect to a Chaser is reached through the prediction (based on a kinematic model of the object) of the velocities of its features. The problem of recovering the pose and the angular rate of the object during occlusions is considered, but no results are shown in case no features are detectable. Besides, when the number of detected features decreases, the precision of the estimation drops drastically.

Although the tumbling motion of an object can be accomplished with a pair of COTS cameras through efficient algorithms, one of the main critical points consists of determining the target motion and mass properties in the in presence of occlusions. This paper presents a method to recover the body attitude during occlusion periods: after the attitude recovery, the angular rate estimation is pursued Kalman filtering the recovered quaternions. The proposed method works under the assumption that the relative position of few detected features is known in some reference system, e.g. the one of an approximate CAD model of the target. Angular rate estimation is fundamental for appropriately guiding and controlling the Chaser spacecraft during the docking maneuver.

The work described in this paper has been developed within the CADET research program, which is co-funded by Regione Piemonte and carried out by a consortium of SMEs and research centers. CADET aims at the functional development of major technologies for the capture and removal of space debris. Within this project, the team of Politecnico di Torino is involved in the localization of the center of mass of the reference Targets [25], in the estimation of their rotational dynamic state [26], and in the selection and verification of the Chaser guidance and control strategies, based on an in-the-loop simulator [27].

The present article combines the studies for the determination of the Target's motion and the choice and application of the guidance strategies and control laws for the Chaser. Section 2 describes the mission profile for the capture of the reference Target (H10 body) using a Chaser equipped with a grasping mechanism; Section 3 presents the main concepts regarding the Target motion determination; Section 4 shows the design of the controllers for the Chaser

attitude and relative trajectory with respect to the Target. In Section 5 the results are presented and discussed, while Section 6 concludes the paper with comments and final remarks.

II. Reference mission

The mission profile for the Chaser within the CADET frame can be split into three phases:

- *Observation phase*. Chaser shall maintain the initial hold point in order to allow the Target analysis through a pair of on board cameras. It means that Chaser stays in the hold point defined by the three component (-30, 0, 0) m with respect to the mating point, with a relative velocity Chaser/Target of 0±0.1 m/s. Moreover, the Chaser reaches and maintains a misalignment between its body Frame and the Local Orbital Frame less than 0.1 rad for each axis and the relative angular velocity is close to 0±0.01 rad/s. That ensures that the Target remain in the Field of View of the cameras [28]. This position is held until the motion of the target is estimated.
- *Capture preparation phase*. Chaser shall move and reach the docking axis from the hold point. It shall perform a fly around maneuver in order to intercept the docking axis. The docking axis is individuated in accordance to the estimated motion. The maneuver for carrying out the Chaser on this axis should have an accuracy of at least the 5%.
- *Capture phase*. Chaser shall perform a straight-line maneuver along the docking axis in order to reach the mating point, which is considered as the Target center of mass. This maneuver has to satisfy the mating requirements explained in Table 1. The approach velocity is the relative linear velocity between Chaser and Target along the capture axis. The lateral misalignment is the distance between the mating point and the grasping mechanism in the plane perpendicular to the capture axis. The lateral velocity is the velocity of the Chaser with respect to the Target in the directions perpendicular to the capture axis. The angular misalignment is the difference between the Target attitude and the Chaser attitude expressed in a Target-fixed reference frame as well as the relative angular rate is the angular velocity of the Chaser with respect to the Target in the same frame.

Parameter	Required performance
Approach velocity	<0.03 m/s
Lateral misalignment	<0.2 m
Lateral velocity	<0.05 m/s
Angular misalignment	<1deg
Angular rate	<0.05 deg/s

Table 1: Performance for Docking

The reference mission considers as Target the H10 family spacecraft, the upper stage of Ariane 4 launchers [29]. For the purpose of the paper, H10 element is tumbling around an a priori unknown axis, different form its main inertial axes.

Chaser spacecraft has been completely designed within CADET program and its main features are reported in Table 2. [30].Chaser's mass do not change during the maneuver because the only variations are given by the propellant consumption, negligible compared to the total weight of the spacecraft.

Properties	Value
Mass	800 Kg
Dimensions	1.5 m x 1.5 m x 5 m
Inertia	Ix=420 Kg/m^2
	Iy=1140 Kg/m^2
	Iz=1150 Kg/m^2

Table 2: Chaser properties

III. Estimation of the Target motion parameters and inertial properties

A. Attitude information from features

A reference triad of axes attached to the target is constructed considering the trajectories of the feature points and their relative positions. The orientation of the aforementioned triad is expressed through quaternions. Given three different points that belong to a rigid body in an inertial frame I, one can define two column vectors, $\bar{v}_i$ and $\bar{v}_u$, whose cross product is the vector $\bar{v}_j$, which is perpendicular to both. A third orthogonal column vector, $\bar{v}_k$, can be simply obtained through another cross product between $\bar{v}_i$ and $\bar{v}_j$. Then, the orientation of a body-fixed reference frame D, which is generally different from the principal body-fixed frame B, with respect to the inertial frame I, is given by the following expression:

$$R_{ID} = \left[\frac{\bar{v}_i}{|\bar{v}_i|} \quad \frac{\bar{v}_j}{|\bar{v}_j|} \quad \frac{\bar{v}_k}{|\bar{v}_k|}\right] \in SO(3) \tag{1}$$

The feature coordinates, which are originally measured in a chaser-fixed reference frame, can be expressed in an inertial frame, as the chaser attitude is assumed to be measurable with high accuracy. The three features have to be

always the same. Thus, if not detected directly, their coordinates have to be evaluated through the assumed prior knowledge of the relative positions between all the detectable features.

A non-singular mapping between an element of the $SO(3)$ group and a unit quaternion always exists; one of the four possible ways to calculate the quaternion is as follows:

$$q_{ID} = \begin{bmatrix} \pm\frac{1}{2}\sqrt{1 + R_{11} + R_{22} + R_{33}} \\ \frac{1}{4q_{IDs}}(R_{32} - R_{23}) \\ \frac{1}{4q_{IDs}}(R_{13} - R_{31}) \\ \frac{1}{4q_{IDs}}(R_{21} - R_{12}) \end{bmatrix} \tag{2}$$

In (Eq. 2), R_{ij} is an element of matrix R_{ID} (the inverse of R_{DI}), and q_{IDs} represents the scalar part of the quaternion q_{ID}. This last equation provides evidence that the quaternion $-q_{ID}$ represents the same orientation as q_{ID}. This property allows this representation to be singularity-free; however, the calculation process requires more than one choice to be made. If three particular features of the target body can be always detected and localized with respect to the inertial frame I, a full four dimensional quaternion signal can be obtained. Each component of this signal will show, in general, several discontinuities due to the redundancy of the quaternion parametrization. However, a smooth equivalent signal could be obtained exploiting one of the existent algorithms for that purpose, e.g., the Stanley method [31]. Inducing continuity facilitates the usage of the obtained signal as a surrogate measurement for an appropriate Kalman filter for estimating the body angular rate..

B. Dealing with occlusions

All the methods for guaranteeing the quaternion continuity assume the attitude information always available. Unfortunately, this assumption seems to be excessively strong due to the harsh lighting condition of the space environment. Since temporary losses of vision data are rather probable, the quaternion signal is likely to present several missing samples. The recovery of the relative original signal depends on whether it may be represented as a *sparse* signal or not. A family of techniques belonging to the so-called *compressed sensing* (CS) theory allows sparse signals to be efficiently recovered via the solution of a generally non-linear optimization program.

Given a generic mono-dimensional signal (everything can be extended to the multi-dimensional case) σ, whose noisy observations are collected in s it holds:

$$s = \Gamma\,\sigma + \eta \tag{3}$$

η represents the noise on the observations while Γ is a generic observation matrix which for instance eliminates several samples from the original signal σ. In this last case, Γ would be a rectangular matrix having null columns in correspondence to missing samples of the original signal. i.e. $\Gamma^T\,\Gamma$ would be a diagonal matrix whose j-th eigenvalue is null if corresponds to a time sample at which no measurement is available. Assuming that the original signal is sparse in some domain and that a linear transform exists, it holds:

$$s = \Gamma\Phi c + \eta \tag{4}$$

Φ represents the application of a non-singular linear mapping between the signal and some coefficients c. If the matrix ΓΦ, known as sensing matrix satisfy the so-called *restricted isometry property* (RIP) [32], then an exactly sparse signal is optimally recovered by solving:

$$\underset{\mathrm{c}}{\operatorname{argmin}} \|\mathrm{c}\|_1 \quad \text{subject to} \quad \|s - \Gamma\Phi c\|_2^2 \leq \varepsilon \tag{5}$$

The RIP is essentially satisfied when a submatrix of the sensing matrix have a l_2 norm which is near to be one. Typically, this condition is satisfied also when the sensing matrix is a completely random one. Defining a *penalization parameter* λ, the problem stated in **Errore. L'origine riferimento non è stata trovata.** is completely equivalent, for a certain value of λ, to the following problem known as LASSO [33]:

$$\underset{\mathrm{c}}{\operatorname{argmin}} \frac{1}{2}\|\Gamma\Phi\mathrm{c} - \mathrm{s}\|_2^2 + \lambda\|\mathrm{c}\|_1 \tag{6}$$

The last problem in **Errore. L'origine riferimento non è stata trovata.** can be solved with a variety of algorithms. Herein SALSA [34] is proposed. It is a fast iterative algorithm that solves an equivalent problem in which two new auxiliary variables, namely l and v, are introduced:

$$\underset{\mathrm{c,v}}{\operatorname{argmin}} \frac{1}{2}\|\Gamma\Phi\mathrm{c} - \mathrm{s}\|_2^2 + \lambda\|v - l\|_1 + \frac{\mu}{2}\|c - v\|_2^2 \tag{7}$$

μ is a second penalization parameter reinforcing the equality constraint $c = v$. The core of the algorithm for solving the problem in **Errore. L'origine riferimento non è stata trovata.** is shown below:

- $v_{k+1} = \mathrm{soft}\left(c_k - l_k, \frac{\lambda}{\mu}\right)$
- $c_{k+1} = (\Phi^*\Gamma^*\Gamma\Phi + \mu I)^{-1}(\Phi^*\Gamma^* s + \mu v_k)$
- $l_{k+1} = v_{k+1} - c_{k+1}$
- $k \leftarrow k + 1$

The *soft thresholding function* is a pure denoising operator: once the first argument is less than the second, the function output is zero; otherwise, the output is the first argument decreased by the second. The shown algorithm is a slight modification of the original SALSA. This variation, which considers the presence of the sensing matrix Γ is extensively explained in [26]

The presented approach can be used for recovering each of the quaternion components, under the assumption that they are mostly sparse in some domain. The motion of space debris can be considered as a periodic and slow succession of finite rotations. This holds because debris can be considered mostly free of external torques. Indeed, if a limited period of time is considered, the effect of the environmental torques is practically unobservable, especially when the measured positions of the features are affected by noise. Thus, assuming that each component of the quaternion is sparse in the frequency domain seems to be more than reasonable. This means that a possible candidate for the linear transformation represented by the matrix Φ may be the inverse discrete Fourier transform (IDFT):

$$\Phi_{\mathrm{ab}} = e^{i\frac{2\pi}{m}ab} \tag{8}$$

being m the dimension of the coefficient vector c.

In a first instance, the generic measurements s in (4) are replaced with q_{IDs}, i.e. the indirectly measured scalar part of the attitude quaternions. The recovery of each measured component of q_{ID} is addressed separately but in parallel remembering that at the end of the procedure the complete recovered quaternion must be re-normalized. Indeed, the recovery do not consider constraints on the norm of the recovered signal.

The mentioned recovery presents a main challenge that do not allows for the standard application of the SALSA algorithm on the complete measured signal. This challenge consists in the presence of missing samples on the measured signal. The entire components of the quaternions appear piece-wise, preventing the application of the aforementioned rules to guarantee continuity between the separated parts of the measured signal. This problem undermines the assumption of *sparsity* of the raw measurements. On the other hand, those rules applies separately to each of the different parts. Then, this paper proposes a method to patch appropriately the various parts in order to pursue an efficient final recovery.

The procedure starts collecting and recovering the first 5 parts of the signal, which are supposed to be separated by many missing samples. It is assumed that each part contains at least 8 samples. If this last assumptions appears not consistent for particular application conditions (very fast tumbling for instance), it is possible to collect a few other

parts. If the total number of measured samples is very low, the success of this first recovery cannot be assured with high confidence.

Considering all the N acquired parts, there is the possibility of managing the signal to obtain 2^{N-1} new signals having the same meaning in terms of attitude information. Indeed, except for the first part of the signal, it is possible to modify the sign of all the samples of each of the remaining parts so that the continuity of the part remains preserved. Hence, the algorithm to solve (7) can be applied to all the obtained signals. An illustrative example of this procedure is given in Fig. 1

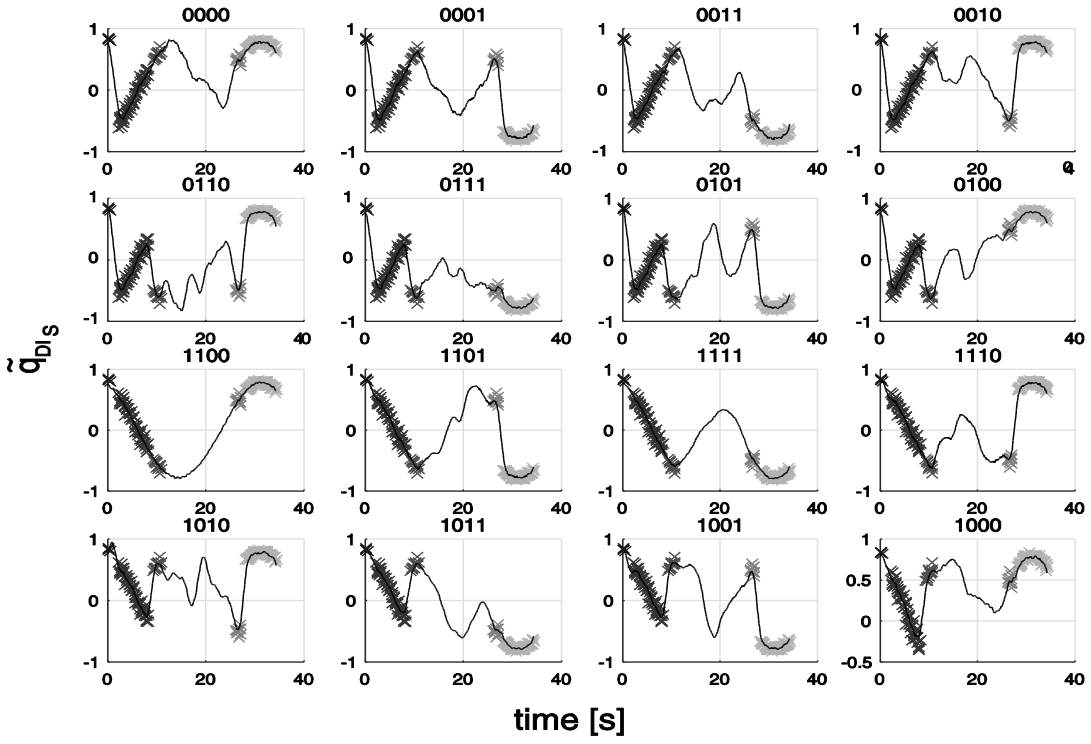

Fig. 1: several equivalent combinations of a measured scalar part of attitude quaternions. Crosses indicates the managed raw data while solid lines correspond to signals recovered with SALSA

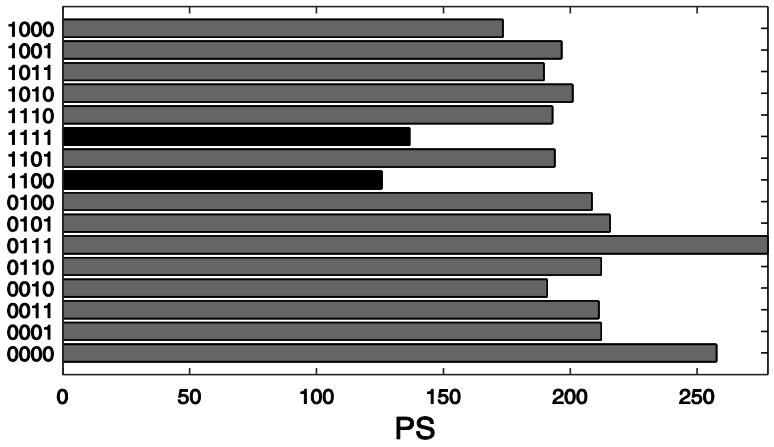

Fig. 2: Sparsity of the recovered scalar parts. Sparsest solutions corresponds to signals labeled with 1111 and 1100

Figure 1 shows the recovery of 16 equivalent scalar parts of measured q_{ID}. Each signal presents a label of 4 digits that shows its relationship with the original raw signal: 0000 corresponds to the original signal, while 1111 indicates that all the signs of q_{IDs} have been changed. Note that only two recovered signals seem really sparse.

To quantify this sparsity, one can choose some numerical score for each recovered signal $\tilde{q}_{ID}$. Herein the following score is proposed:

$$PS = k_0\|c\|_0 + k_1\|c\|_0 \tag{9}$$

where k_0 and k_1 are appropriate scaling constant. The computed scores for signals in Fig.1 are resumed in Fig. 2 through a histogram.

From the 16 recovered signal only the best two hold. Hence, it is possible to collect new measured samples until a new occlusion occurs. An illustrative example of this collection and of the consequent sign adjustments is in Fig. 3.

The recovery of all the 4 resulting equivalent signals can be pursued another time with SALSA. The procedure repeats for an undefined number of acquired parts of the quaternions, each separated by many missing samples. For each repetition, all the past-acquired data are exploited; clearly, after few iterations (e.g. 4 or 5) only the best combination of the past pieces is considered, maintaining limited the computational effort.

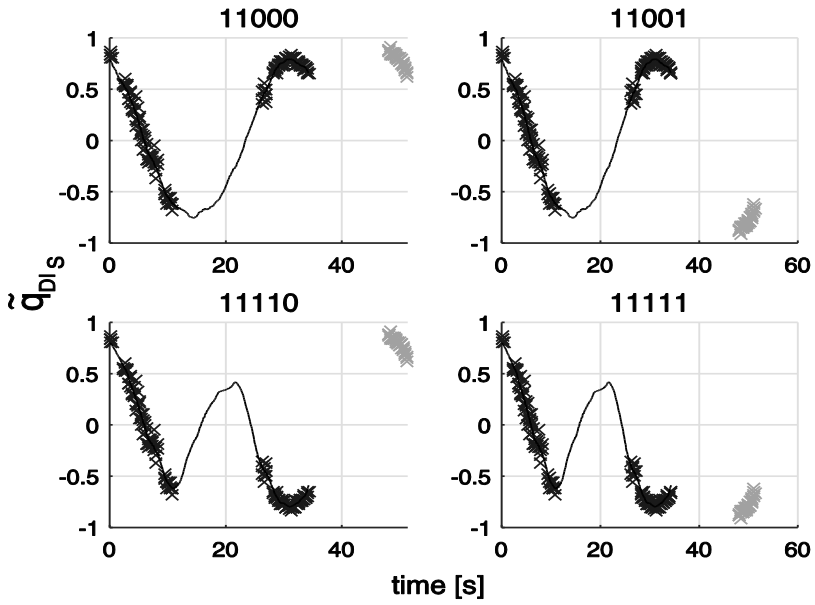

Fig. 3: After holding the best recovered signals, a new raw part is considered with both the signs of all its samples

Unfortunately, the presented approach cannot strictly work in real-time due to the necessity of patching appropriately the pieces of the signal, which is interrupted by several missing parts. However, each recovery step provides a partial signal that could be exploited for further computations.

The peculiar redundancy of the quaternions introduces another issue: the recovered quaternions are useful to observe the dynamics of the target through Kalman filtering techniques. In the case of sparse measurements, Kalman filtering and compressive sampling techniques can be combined optimally in a unique fashion. One valuable work that treat this topic in a general technical context is in [35]. However, these valid approaches are not applicable in the specific case examined in this paper. Indeed, the sparsity of the measurements depends strictly on the choices made on all the measured samples regarding their sign. As explained in this section, due to the occurrence of occlusions, the final choice regarding the signs of the samples of each new acquired part is made *a posteriori*, once all the possible combinations of the other parts have been already recovered.

Hence, thought this is not a perfect solution, the best possibility to estimate the complete dynamic state of the target is represented by the usage of a Kalman filter immediately after the attitude recovery procedure.

C. Estimation of angular rate and inertia ratios

The Target attitude information is typically useful to understand its dynamic state, which comprises the angular rate and at least a normalized form of the body inertia tensor. As the object is practically a torque-free body, the actual values of the principal inertia moments are not observable, but their relative magnitudes are still observable. An Unscented Kalman filter [36] is here proposed for that purpose. The discrete state-space system is the following:

$$\begin{aligned} x_k &= \begin{bmatrix} q_{IB_{tg}} \\ \omega_{IB_{tg}} \\ I_{B_{tg}} \\ q_{BD_{tg}} \end{bmatrix}_k \quad ; \quad x_{k+1} = x_k + t \begin{bmatrix} \frac{1}{2}\ \omega_{IB}{}^{\dagger}_{tgk}\, q_{IB_{tgk}} \\ \mathrm{diag}(I_{B_{tgk}})^{-1} \left(\omega_{IB_{tgk}} \times \mathrm{diag}(I_{B_{tgk}})\, \omega_{IB_{tgk}} \right) \\ 0 \\ 0 \end{bmatrix} + w_k \\ z_k &= \tilde{q}_{ID_k} \quad ; \quad z_k = q_{BD_{tgk}} \otimes q_{IB_{tgk}} + n_k \end{aligned} \tag{10}$$

In **Errore. L'origine riferimento non è stata trovata.**, t is the time step, $q_{IB_{tg}}$ is the attitude quaternion of a principal body-fixed frame B with respect to the inertial frame, $\omega_{IB_{tg}}$ is the absolute body angular rate expressed in the frame B, $I_{B_{tg}}$ is a normalized vector containing the three principal inertia ratios, and $q_{BD_{tg}}$ is a constant offset quaternion that rotates the frame B into the generic body-fixed frame D. w and n identify respectively the process and the measurement noise vectors. The symbol $\otimes$ identifies quaternion multiplication while $\omega_{IB_{tg}}{}^{\dagger}$ corresponds to the following skew-symmetric matrix:

$$\omega_{IB_{tg}}{}^{\dagger} = \begin{bmatrix} 0 & -\omega_{IB_{tg}{}_x} & -\omega_{IB_{tg}{}_y} & -\omega_{IB_{tg}{}_z} \\ \omega_{IB_{tg}{}_x} & 0 & \omega_{IB_{tg}{}_z} & -\omega_{IB_{tg}{}_y} \\ \omega_{IB_{tg}{}_y} & -\omega_{IB_{tg}{}_z} & 0 & \omega_{IB_{tg}{}_x} \\ \omega_{IB_{tg}{}_z} & \omega_{IB_{tg}{}_y} & -\omega_{IB_{tg}{}_x} & 0 \end{bmatrix} \tag{11}$$

The presence of the offset quaternion $q_{BD_{tg}}$ in the state has been already considered in [17]. It is necessary to estimate correctly the inertia moments. Actually, the second equation in (10), which comes from the Euler's equation, would be valid also if both the angular rate and the angular momentum were expressed in any body-fixed reference system (D included). Notwithstanding, if the reference system remains generic, it is necessary to estimate the entire inertia tensor. Thus, it arises that the observer could also find a diagonal inertia tensor such that the estimated attitude would match the recovered $\tilde{q}_{DI}$. However, this inertia tensor would be the one of a different body from the considered target. Instead, the expression of the angular rate in a principal body-fixed frame constraints the estimated inertia tensor to be diagonal. Thus, the observer can permute only the numerical order of the three principal moments.

Due to this possible permutations the observable values of q_{DB} are non-unique, but there are only 6 possible rotations that maps the attitude of the 6 possible principal reference triads. Moreover, any of the possible solutions have the same practical validity.

Following a similar procedure to the one exposed in [37] for a different estimation problem, we linearized the equations in (10) with respect to the considered state variables. Then, after considering random linearization points, under the unitary norm constraints for quaternions and inertia ratios, many local observability matrices were evaluated. The computed rank for those matrices was always 11. If $q_{BD_{tg}}$ is considered known, that is equivalent to directly measure $q_{IB_{tg}}$, the rank becomes 9 against 10 unknown variables: this condition is due to the non-observability of the absolute values of the inertia moments. With the introduction of $q_{BD_{tg}}$ in the unknown variables, it is necessary to know two of the three moments of inertia to gain an equivalent condition (rank 11 against 12 unknowns).

Actually, the introduced ambiguity does not regard the three values of the principal inertia moments but only their order within the state vector. However, as already mentioned, this is not a real problem because the found $q_{BD_{tg}}$ and $q_{IB_{tg}}$ would remain always consistent with the found order. Hence, for instance, one can express the observed angular rate in the inertial frame *I* thus to remove any ambiguity about the motion of the target. The numerical results shown later on will reflect those considerations.

For each time step, the Kalman loop can be performed until the inertia ratios converge to stable values. To determine this moment the variances of the inertia ratios in a moving time window could be evaluated. Once the biggest of these variances is smaller than a reasonable tolerance, the algorithm terminates. The resulting inertia ratios are useful to understand the mass distribution of the object and the location of the principal axes of inertia.

Unscented Kalman filtering is an effective way for estimating the state of systems having a non-linear dynamics. Some *sigma* points in the state space are chosen based on the prior knowledge of the state covariance and of the expected value of the state. All the points are propagated undergoing the non-linear model of the system in order to predict a new weighted expected value and a new related covariance. Given the generic non-linear state-space equations:

$$\begin{aligned} x_{k+1} &= f(x_k) + w_k \\ z_k &= h(x_k) + n_k \end{aligned} \tag{11}$$

If the state has dimension L a number of $2L + 1$ sigma points χ_i are evaluated and propagated in accordance with the state covariance P_k and x_k [38]. The a-priori expected measurements at the instant $k + 1$, which are associated to these sigma points, are the so called innovations:

$$\zeta_{i,k+1|k} = h\left(\chi_{i,k+1|k}\right) \qquad \forall\, i = 0, 1, \dots, 2L \tag{12}$$

Two covariance matrices, the innovation covariance P_{zz_k} and the cross covariance P_{xz_k}, can be then evaluated for computing the Kalman Gain

$$K_k = P_{xz_k}\ P_{zz_k}^{-1} \tag{13}$$

The classic additive updating stage of the Kalman loop typically does not preserve the unitary norm of the quaternions. For that reason, the quaternions in the state vector are renormalized after each updating stage. This *brute-force* approach is not the most elegant one but is proven to work quite well [39], [40].

IV. Chaser guidance and control strategies

The chosen guidance and control strategies in the CADET mission are presented in this Section. In order to define the strategies, it is important to establish the adopted reference frames:

- The ECEF (Earth Centered Earth Fixed) frame is considered a quasi-inertial frame for the mission and it has origin O_{ecef} in the centre of the Earth, x_{ecef} in the equatorial plane, pointing toward the mean of the vernal equinox; y-axis in the equatorial plane, such that $z_{ecef} = x_{ecef} \times y_{ecef}$; and z_{ecef} is normal to the equatorial plane and pointing north.
- The Spacecraft Local Orbital frame has its origin O_o in the center of mass of the spacecraft; xo is defined such that $x_o = y_o \times z_o$ (x_o is in the direction of the orbital velocity vector but not necessarily aligned with it), y_o is in the opposite direction of the angular momentum vector of the orbit and z_o is radial from the spacecraft CoM to the centre of the Earth. In this paper, both the Target Local Orbital (x_{otg}, y_{otg}, z_{otg}) frame and the Chaser Local Orbital frame (x_{och}, y_{och}, z_{och}) are taken into account.
- The Target Body frame has origin *O*tg in the Target centre of mass, the direction of the axes depending on the Target motion and $z_{tg} = x_{tg} \times y_{tg}$ forming a right handed system.

- The Chaser Body frame has origin O_{ch} in the Chaser centre of mass, the direction of the axes depending on the Target motion and $z_{ch}= x_{ch} \times y_{ch}$ forming a right handed system. It is to remark that x_{ch} is the axis on which are mounted both the docking mechanism and the cameras system.

A. Guidance strategies

Taking into account the phases described in Section 2, three guidance strategies for each final approach phase have been identified:

- During the *Observation phase*, the Chaser maintains the initial hold point and mounted cameras point the Target. In particular the desired position values are the coordinates of the hold point (-30 0 0) in the Target Local Orbital frame and the desired alignment of the Chaser body frame with the Chaser orbital frame is expressed by the quaternion q_{des}=[0 0 0 1].
- During the *Capture preparation phase* a first fly-around maneuver leads the Chaser to intercept the capture axis maintaining the docking system pointing the Target. The desired final values for this phase are defined by the point of the individuated docking axis that is distant 30 m from the Target CoM. The desired attitude is defined so that the docking mechanism points the Target: it means that the x_{ch} axis shall be aligned with the docking axis.
- During the *Capture phase*, a straight-line maneuver brings the Chaser to the docking point. The desired final position is the docking point that is coincident with O_{tg}. The desired attitude is defined as for the previous phase.

All the guidance strategies follow a closed loop deceleration profile.

B. Controllers design

In order to guarantee that the Chaser attitude and relative position with respect the Target follows the desired values for each phase, a *Model Predictive Controller* have been designed.

1. Model predictive control laws

Model Predictive Control (MPC) is a modern control technique, which allows taking into account future value prediction of the state space. MPC is based on the optimization criterion defined as:

$$J\big(U(k),x(k|k)\big) = \sum_{i=0}^{H_p-1} L\big(x(k+i|k),U(k+i|k)\big) + \Phi_{\mathrm{W}}\left(x\big(k+H_p|k\big)\right) \quad (14)$$

where H_p is the prediction horizon, $L(.)$ is the weighting function, $\Phi_{\mathrm{W}}\big(x(k|k)\big)$is the terminal state weighting function, and $x(k|k)$ is the state measurement at time k and U(k+1|k) is the control action at time k+1 given k. In particular, the weighting functions are characterized by:

$$L(x,u) = x^T Q x + u^T R u \quad (15)$$

$$\Phi_{\mathrm{W}}\big(x(k|k)\big) = x^T P x \quad (16)$$

where Q, R and P are symmetric positive definite matrices.

Substituting **Errore. L'origine riferimento non è stata trovata.** and **Errore. L'origine riferimento non è stata trovata.** in **Errore. L'origine riferimento non è stata trovata.**, the optimization criterion can be written as:

$$J\big(U(k),x(k|k)\big) = \sum_{i=0}^{H_p-1} x(k+i|k)^T Q x(k+i|k) + u(k+i|k)^T R u(k+i|k) + x\big(k+H_p|k\big)^T P x\big(k+H_p|k\big) \quad (17)$$

In order to set the optimization problem in a quadratic formulation, **Errore. L'origine riferimento non è stata trovata.** can be rewritten as:

$$J\big(U(k),x(k|k)\big) = \tfrac{1}{2} X(k)^T \mathcal{Q} X(k) + U(k) \mathcal{R} U(k) \quad (18)$$

where:

$$X(k) = \begin{bmatrix} x(k|k) & x(k+2|k) & \dots & x\big(k+H_p|k\big) \end{bmatrix}$$

$$U(k) = \begin{bmatrix} u(k|k) & u(k+1|k) & \dots & u\big(k+H_p-1|k\big) \end{bmatrix}$$

$$\mathcal{R} = \begin{bmatrix} R & \dots & 0 \\ \dots & \dots & \dots \\ 0 & \dots & R \end{bmatrix} \qquad \mathcal{Q} = \begin{bmatrix} Q & \dots & 0 \\ \dots & \dots & \dots \\ 0 & \dots & Q \end{bmatrix}$$

MPC control requires the prediction of the future states until the prediction horizon H_p. This is possible thanks to the augmented system described by:

$$X(k) = \mathcal{A} x(k|k) + \mathcal{B} U(k) \quad (19)$$

where:

$$\mathcal{A} = \begin{bmatrix} A & A^2 & \dots & A^{H_p} \end{bmatrix}^T \qquad \mathcal{B} = \begin{bmatrix} B & 0 & \dots & 0 & 0 \\ AB & B & \dots & 0 & 0 \\ \dots & \dots & \dots & \dots & \dots \\ A^{H_p-2}B & A^{H_p-1}B & \dots & B & 0 \\ A^{H_p-1}B & A^{H_p-2}B & \dots & A^2B & AB \end{bmatrix}$$

The cost functions of MPC taken into account the predictions are obtained substituting **Errore. L'origine riferimento non è stata trovata.** in **Errore. L'origine riferimento non è stata trovata.**:

$$J\big(U(k),x(k|k)\big) = [\mathcal{A}x(k|k) + \mathcal{B}U(k)]^T\mathcal{Q}[\mathcal{A}x(k|k) + \mathcal{B}U(k)] + U(k)\mathcal{R}U(k) = [x(k|k)^T\mathcal{A}^T\mathcal{Q}\mathcal{A}x(k|k) +$$

$$U(k)^T[\mathcal{B}^T\mathcal{Q}\mathcal{B} + \mathcal{R}]U(k) + 2x(k|k)^T\mathcal{A}^T\mathcal{Q}\mathcal{B}U(k)] = U(k)^TH_{opt}U(k) + x(k|k)^TF_{opt}U(k) + \bar{J}\big(x(k|k)\big) \quad (20)$$

where $H_{opt} = \mathcal{B}^T\mathcal{Q}\mathcal{B} + \mathcal{R}$; $F_{opt} = 2\mathcal{A}^T\mathcal{Q}\mathcal{B}$

The final formulation of the control problem is a constrained optimization problem, which must be solved at each time step:

$$\begin{cases} \min J\big(U(k),x(k|k)\big) J = \min U(k)^TH_{opt}U(k) + x(k|k)^TF_{opt}U(k) \\ s.t. \\ x(k+1|k) = Ax(k|k) + Bu(k): \\ U(k) \in \mathbb{U} \\ x(k+i|k) \in \mathbb{X},\ i = 1,2,\dots,H_p \\ x\big(k+H_p|k\big) \in \mathbb{X}_F \subset \mathbb{X} \end{cases} \quad (21)$$

where $\mathbb{U}$, $\mathbb{X}$ and $\mathbb{X}_F$ are respectively the input constraint set, sate constraint set and terminal constraint set. Considering a quadratic criterion and a linear constraint set, the optimization problem becomes a quadratic programming problem. The control is applied via the Receding Horizon Principle, which is based on the following procedure at each time step:

- To get the state $x(k)$
- To solve the optimization problem to find the solution $U^o(k) = [u^o(k|k) \quad u^o(k+1|k) \quad \dots \quad u^o(k+H_p|k)]$
- To apply the control action $u(k) = u^o(k,k)$

2. Tracking Model predictive control

The tracking model prediction control optimizes the reference tracking: in this sense, the optimization criterion **Errore. L'origine riferimento non è stata trovata.** should be modified introducing the reference vector r(k) for the prediction.

$$J\big(U(k),x(k|k)\big) = \sum_{i=0}^{H_p-1}\big(x(k+i|k) - r(k+i)\big)^TQ\big(x(k+i|k)^T - r(k+i)\big) + u(k+i|k)^TRu(k+i|k) \quad (22)$$

Considering the augmented system **Errore. L'origine riferimento non è stata trovata.** and introducing the augmented reference vector $R(k) = [r(k) \quad r(k+1) \quad \dots \quad r(k+H_p)]$, **Errore. L'origine riferimento non è stata trovata.** can be rearranged as:

$$J\big(U(k),x(k|k)\big) = [\mathcal{A}x(k|k) + \mathcal{B}U(k) - R(k)]^T \mathcal{Q}[\mathcal{A}x(k|k) + \mathcal{B}U(k) - R(k)] + U(k)\mathcal{R}U(k) =$$

$$[x(k|k)^T \mathcal{A}^T \mathcal{Q}\mathcal{A}x(k|k) + U(k)^T[\mathcal{B}^T\mathcal{Q}\mathcal{B} + \mathcal{R}]U(k) + 2x(k|k)^T\mathcal{A}^T\mathcal{Q}\mathcal{B}U(k) - 2R(k)^T\mathcal{Q}\mathcal{A}x(k|k) +$$

$$2R(k)^T\mathcal{Q}\mathcal{B}U(k) + R(k)^T\mathcal{Q}R(k)] \tag{23}$$

Substituting

$$H_{opt} = \mathcal{B}^T\mathcal{Q}\mathcal{B} + \mathcal{R} \quad ; \qquad F_{opt} = 2\begin{bmatrix}\mathcal{A}^T\mathcal{Q}\mathcal{B} \\ \mathcal{Q}\mathcal{B}\end{bmatrix}$$

the optimization criterion becomes a quadratic formulation described by:

$$J\big(U(k),x(k|k)\big) = U(k)^T H_{opt} U(k) + \begin{bmatrix}x(k|k) \\ R(k)\end{bmatrix}^T F_{opt} U(k) + \bar{J}\big(x(k|k),R(k)\big) \tag{24}$$

Errore. L'origine riferimento non è stata trovata. is the cost function that substitutes the **Errore. L'origine riferimento non è stata trovata.**.

C. MPC for the Chaser trajectory

The controllers design starts from the definition of the system that has to be controlled: in particular, it is crucial to explain the equations that describe the relationships between the Target and the Chaser motions and the equation of the Chaser attitude dynamics and kinematics.

Thanks to the actual initial relative position and the maneuver time, it is possible to consider the approach as a circular orbit and evaluate the relative position and velocity between Chaser and Target through the Hill's equations as:

$$\begin{aligned} \ddot{\rho_x} - 2\theta\,\dot{\rho_z} &= \Delta\gamma_x \\ \ddot{\rho_y} + \theta^2\rho_y &= \Delta\gamma_y \\ \ddot{\rho_z} + 2\theta\dot{\rho_x} - 3\theta^2\rho_z &= \Delta\gamma_z \end{aligned} \tag{25}$$

where ρ_x, ρ_y, ρ_z determine the relative Chaser position, θ is the angular frequency of the Target orbit, and $\Delta\gamma_i$ represent the sum of the disturbance (i.e. aerodynamic force, solar pressure, J2 orbital perturbation,)and control forces. This formulation of the Hill's equations allows reproducing the maneuver approach of the Chaser with respect to an arbitrary axis.

The MPC design starts from the linearization of these equations that can be represented in the state space form as:

$$\dot{x}(t) = A(t)x(t) + Bu(t) \tag{26}$$

where x(t) = $[\rho_x\ \rho_y\ \rho_z\ \dot{\rho_x}\ \dot{\rho_y}\ \dot{\rho_z}]$ is the state vector constituted by the three components of the Chaser position and the velocity with respect to the Target frame, u(t)=[F_{cx} F_{cy} F_{cz}] is the vector of the control forces given by the thrusters, and A and B are defined as follow

$$A = \begin{bmatrix} 0 & 0 & 0 & 1 & 0 & 0 \\ 0 & 0 & 0 & 0 & 1 & 0 \\ 0 & 0 & 0 & 0 & 0 & 1 \\ 0 & 0 & 0 & 0 & 0 & 2\theta^2 \\ 0 & -\theta^2 & 0 & 0 & 0 & 0 \\ 0 & 3\theta^2 & 0 & -2\theta^2 & 0 & 0 \end{bmatrix} \qquad B = \begin{bmatrix} 0 & 0 & 0 \\ 0 & 0 & 0 \\ 0 & 0 & 0 \\ \frac{1}{m_c} & 0 & 0 \\ 0 & \frac{1}{m_c} & 0 \\ 0 & 0 & \frac{1}{m_c} \end{bmatrix}$$

In order to maintain the computational cost acceptable, within the selected time step of 0.5 seconds, a prediction horizon of four is employed.

The next step is the tuning of the MPC weighting matrices Q and R using an approach "trial and error" that leads to the final definition.

$$Q = \begin{bmatrix} 10 & 0 & 0 & 0 & 0 & 0 \\ 0 & 10 & 0 & 0 & 0 & 0 \\ 0 & 0 & 10 & 0 & 0 & 0 \\ 0 & 0 & 0 & 1000 & 0 & 0 \\ 0 & 0 & 0 & 0 & 1000 & 0 \\ 0 & 0 & 0 & 0 & 0 & 1000 \end{bmatrix} \qquad R = \begin{bmatrix} 0.25 & 0 & 0 \\ 0 & 0.25 & 0 \\ 0 & 0 & 0.25 \end{bmatrix}$$

With the command constraint given by the thrusters saturation $u_{max} = [8,\ 8,\ 8]$.

D. MPC for the Chaser attitude

This section shows the design process for the Chaser attitude controller. For the purpose of the mission, it is possible to assume that the Target orbital local frame and the Chaser orbital local frame are oriented in the same way because the distance between the spacecraft is very small with respect to the orbit.

The starting point is the definition of the Chaser attitude dynamics and kinematics equation. The dynamics of the attitude of a satellite is based on rigid bodies' dynamics which gives the angular speed of the Chaser with respect to ECEF frame:

$$\dot{\omega}_{IB_{ch}} = T_{Bch} - I_{Bch}^{-1}\omega_{IB_{ch}} \times I_{B_{ch}}\omega_{IB_{ch}} \tag{27}$$

where T_{Bch} is the sum of the torques acting on the Chaser (i.e. aerodynamic torque, solar pressure torque, gravity gradient torque, torque generated internal residual magnetic field), $I_{B_{ch}}$ is the inertia matrix of the Chaser, $\omega_{IB_{ch}}$ is the angular velocity of the Chaser with respect to the inertial frame expressed in the body frame.

The Chaser angular velocity with respect to the orbital local frame, $\omega_{OB_{ch}}$, is:

$$\omega_{OB_{ch}} = \omega_{IB_{ch}} - R_{OB_{ch}}^{T}\omega_{IO_{ch}} \tag{28}$$

where $\omega_{IO_{ch}}$is the angular velocity of the orbital frame with respect to the inertial frame and

$R_{OB} = \begin{bmatrix} q_{obs}^2 + q_{\mathrm{ob1}}^1 - q_{\mathrm{ob2}}^2 + q_{\mathrm{ob3}}^2 & 2(q_{\mathrm{ob1}}q_{\mathrm{ob2}} + q_{\mathrm{ob3}}q_{sob}) & 2(q_{\mathrm{ob1}}q_{\mathrm{ob3}} - q_{\mathrm{ob2}}q_{obs}) \\ 2(q_{\mathrm{ob1}}q_{\mathrm{ob2}} - q_{\mathrm{ob3}}q_{obs}) & -q_{\mathrm{ob1}}^2 + q_{\mathrm{ob2}}^2 - q_{\mathrm{ob3}}^2 + q_{obs}^2 & 2(q_{\mathrm{ob2}}q_{\mathrm{ob3}} + q_{obs}q_{\mathrm{ob1}}) \\ 2(q_{\mathrm{ob1}}q_{\mathrm{ob3}} + q_{\mathrm{ob2}}q_{obs}) & 2(q_{\mathrm{ob2}}q_{\mathrm{ob3}} - q_{\mathrm{ob1}}q_{obs}) & -q_{\mathrm{ob1}}^2 - q_{\mathrm{ob2}}^2 + q_{\mathrm{ob3}} + q_{obs}^2 \end{bmatrix}$, and $q_{OB} =$

$[q_{OBS} \quad q_{\mathrm{OB1}} \quad q_{\mathrm{OB2}} \quad q_{\mathrm{OB3}}]^T$ represent the attitude of the Chaser with respect to the orbital frame.

The attitude kinematic equations are expressed by:

$$\dot{q}_{OB_{ch}} = \left[\mathrm{Q}_{\mathrm{OB}_{ch}}\right]\omega_{IB_{ch}} \tag{29}$$

where:

$$\left[\mathrm{Q}_{\mathrm{OB}_{ch}}\right] = \begin{bmatrix} -\mathrm{q}_{\mathrm{ob1}} & -q_{\mathrm{ob2}} & -q_{\mathrm{ob3}} \\ q_{obs} & q_{\mathrm{ob3}} & -q_{\mathrm{ob2}} \\ -q_{\mathrm{ob3}} & q_{obs} & q_{\mathrm{ob1}} \\ q_{\mathrm{ob2}} & -q_{\mathrm{ob1}} & q_{obs} \end{bmatrix}$$

The first step in the control design is the linearization of these equations about the current quaternion and angular rate estimation. A representation as in (26) can be obtained, where $x = [q_{OB_s} \quad q_{OB_1} \quad q_{OB_2} \quad q_{OB_3} \quad \omega_{IB_x} \quad \omega_{IB_y} \quad \omega_{IB_z}]^T$, u is the control torques given by the thrusters, and

$$A = \begin{bmatrix} 0_{4x3} & [Q_{OBch}] \\ 0_{3x3} & \begin{bmatrix} 0 & \frac{\omega_{\mathrm{IB_z}}(\mathrm{I_y} - \mathrm{I_z})}{\mathrm{I_x}} & \frac{\omega_{\mathrm{IB_y}}(\mathrm{I_y} - \mathrm{I_z})}{\mathrm{I_x}} \\ -\frac{\omega_{\mathrm{IB}_z}(\mathrm{I_x} - \mathrm{I_z})}{\mathrm{I_y}} & 0 & -\frac{\omega_{\mathrm{IB_x}}(\mathrm{I_x} - \mathrm{I_z})}{\mathrm{I_y}} \\ \frac{\omega_{\mathrm{IB_y}}(\mathrm{I_x} - \mathrm{I_y})}{\mathrm{I_z}} & \frac{\omega_{\mathrm{IB_x}}(\mathrm{I_x} - \mathrm{I_y})}{\mathrm{I_z}} & 0 \end{bmatrix} \end{bmatrix}, \quad B = \begin{bmatrix} 0 & 0 & 0 \\ 0 & 0 & 0 \\ 0 & 0 & 0 \\ 0 & 0 & 0 \\ \frac{1}{2I_x} & 0 & 0 \\ 0 & \frac{1}{2I_y} & 0 \\ 0 & 0 & \frac{1}{2I_z} \end{bmatrix}$$

The next step is the manual tuning of the MPC weighting matrices Q and R using an approach "try and error" that leads to the final definition:

$$Q = \begin{bmatrix} 300 & 0 & 0 & 0 & 0 & 0 & 0 \\ 0 & 300 & 0 & 0 & 0 & 0 & 0 \\ 0 & 0 & 300 & 0 & 0 & 0 & 0 \\ 0 & 0 & 0 & 300 & 0 & 0 & 0 \\ 0 & 0 & 0 & 0 & 200 & 0 & 0 \\ 0 & 0 & 0 & 0 & 0 & 200 & 0 \\ 0 & 0 & 0 & 0 & 0 & 0 & 200 \end{bmatrix}, R = \begin{bmatrix} 0.004 & 0 & 0 \\ 0 & 0.004 & 0 \\ 0 & 0 & 0.004 \end{bmatrix}$$

with the constraints given by the thruster saturation $u_{max} = [4 \quad 4 \quad 4]^{T}$.

V. Results

In order to test the proposed methodologies, the motions of the target and of the chaser spacecraft have been simulated with typical mathematical models. In particular, Euler equations have governed the relative attitude motion. Environmental perturbations and gravity gradient torque have been added to the model (see, for instance, [41] for more details). The Chaser has been positioned on the initial hold point with an attitude with respect to its own orbital frame that is expressed by the quaternion (0 0 0 1). The inertial properties of the target, the initial components of the angular rate in principal body axes, and the initial attitude quaternions are shown in Table 3. These values have been chosen in accordance with the characteristics of the considered removal mission, but they have been arbitrarily selected from a set of plausible values. Therefore, they are completely general from the algorithm's point of view.

Parameter	Value	Normalized Value
$\boldsymbol{I_{B_{tgx}}}$	9000 kg · m^2	0.2562
$\boldsymbol{I_{B_{tgy}}}$	23200 kg · m^2	0.6604
$\boldsymbol{I_{B_{tgz}}}$	24800 kg · m^2	0.7059
$\boldsymbol{\omega_{IB_{tgx}}(0)}$	0.150 rad/s	0.9994
$\boldsymbol{\omega_{IB_{tgy}}(0)}$	0.053 rad/s	0.0353
$\boldsymbol{\omega_{IB_{tgz}}(0)}$	0 rad/s	0
$\boldsymbol{q_{IB_{tgS}}(0)}$	−0.0220 rad	--
$\boldsymbol{q_{IB_{tg1}}(0)}$	0.0405 rad	--
$\boldsymbol{q_{IB_{tg2}}(0)}$	0.7349 rad	--
$\boldsymbol{q_{IB_{tg3}}(0)}$	0.6766 rad	--
$\boldsymbol{q_{DB_{tgS}}}$	−0.0022 rad	--
$\boldsymbol{q_{DB_{tg1}}}$	0.0424 rad	--
$\boldsymbol{q_{DB_{tg2}}}$	0.0734 rad	-
$\boldsymbol{q_{DB_{tg3}}}$	0.9964 rad	

Table 3: Initial Target conditions

The positions of some features of the Target were calculated for each sample time of the motion simulation in order to obtain their trajectories. It is important to note that in real contexts each of the features of the objects could have the possibility of exiting from the FOV of the sensors for several time intervals.

For that reason, the trajectory of each feature is not calculated for the whole period of the simulation but only for the time windows in which it is supposed into the FOV of the passive sensors. In particular, a feature is supposed to be into the FOV if its position vector and the normal to the Target surface in the point form an acute angle. This idea is

typical in the field of computer graphics for removing hidden surfaces of represented objects. In particular, the related technique is known as backface culling [42].

A white Gaussian noise with zero mean and 50 mm standard deviation has been added finally to the three coordinates of each feature. This value comes from the simulation of the feature tracking via a stereo-rig system. The chosen measurement model is similar to the ones in [23] and in [43]. In particular, the perspective projection π has been considered for each of the two cameras composing the stereo-rig:

$$\pi\left({}^{S}\rho_f\right) = {}^{S}\begin{bmatrix}\frac{\rho_{f1}}{\rho_{f2}} & \frac{\rho_{f3}}{\rho_{f2}}\end{bmatrix} \tag{30}$$

where ${}^{S}\rho_f$ is the position of a generic feature expressed in the characteristic reference system S of the stereo-rig. The origin of S is placed on the center of projection of the first camera. The first axis of S is aligned with the baseline of the system, whose chosen length is 1 m. The third axis of S is directed upward so that the second axis is oriented toward depth. The projection π has been applied for both the cameras to 10^6 features uniformly distributed inside a 3m×10m×3m box having its center at $[0 \quad 25 \quad 0]$m in the S frame. A white Gaussian noise having zero mean and $5 \cdot 10^{-5}$ standard deviation has been added to the projected points.

After the inverse projection, the differences between the found coordinates and the original uncorrupted ones have been reported in Fig. 1 through three different histograms. From the latter figure the distributions of the errors appear Gaussian-shaped and the standard deviation of the heaviest uncertainty, which is about the depth coordinate,

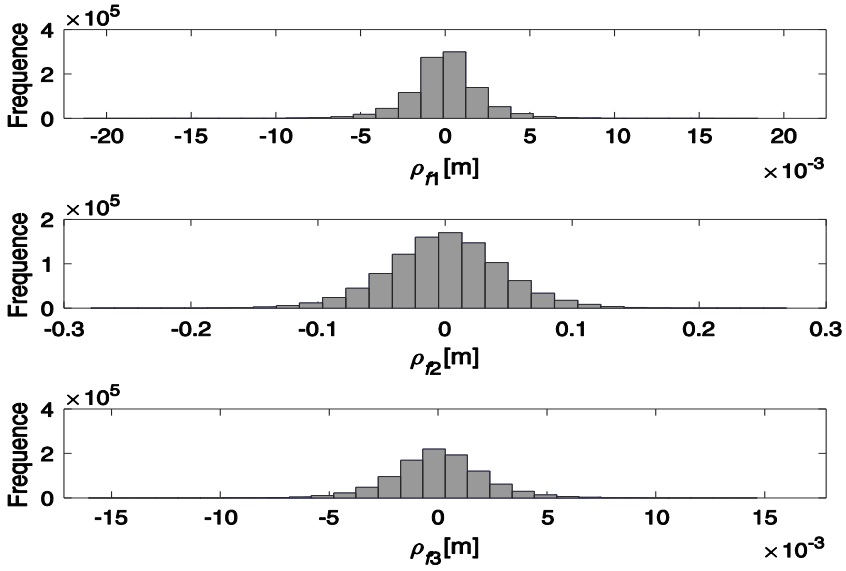

Fig. 4: distribution of the errors on the coordinates of 10^6 features virtually detected at a sample time by a modeled stereo-rig system

amounts to 50 mm. The measured coordinates should be expressed in the inertial frame: this operation is achieved by using a known orthonormal rotation matrix. Thought this matrix is time varying, the maximum standard deviation of the errors for each axis cannot exceed 50 mm due the mentioned orthonormality.

A. Estimation of the dynamic state of the target from simulated data

The first phase of the state estimation consists of the attitude recovery. In Fig. 5 the recovered scalar component of the quaternion $\tilde{q}_{ID}$ is shown together with its raw observations. Missing samples have been optimally recovered with SALSA [33]. In addition, an efficient denoising has been achieved with this technique.

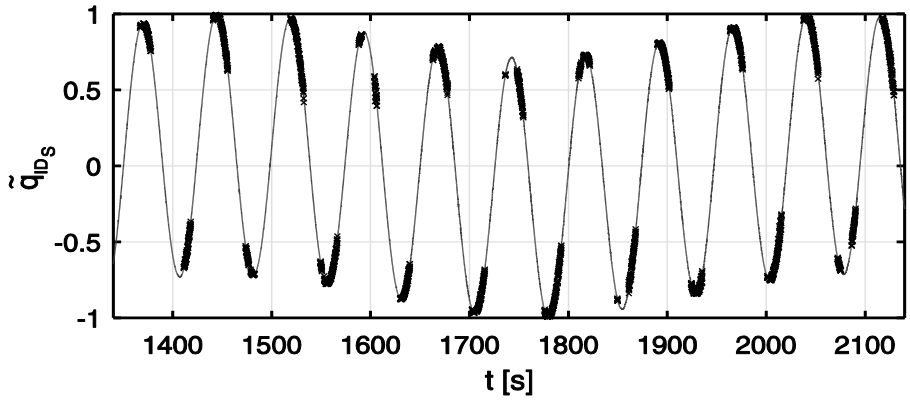

Fig. 5: recovered attitude information and relative corrupted signal

Quaternions are used to feed an unscented Kalman filter to obtain angular rate components with respect to the inertial frame. The efficacy of the estimation is shown in Fig.3where the estimated components are compared with the reference one. The estimated principal normalized moments of inertia are also illustrated inFig.3. The actual absolute magnitude of the volume of the inertia ellipsoid does not influence the attitude motion behavior, so the absolute magnitudes of the inertia moments are obviously unobservable. Fig. 4 and Fig. 5 illustrate the estimated quaternions $q_{IB_{tg}}$ and $q_{BD_{tg}}$. Note from the last figure that in this considered example the found $q_{BD_{tg}}$ coincides with the reference one, so the order of the estimated values of the principal inertia moments within the state vector is the same of the one of the reference values in Table 3. Due to the non-observability issue introduced by $q_{BD_{tg}}$, the found offset quaternions could have been different from the reference one, but not the values of the normalized inertia moments, whose order, however, would have resulted exchanged. This issue can only provide graphical difficulties in presenting the results due, for example, to the permutation of all the components of the angular rate. From the technical point of view no

difficulties occur because the complete estimated state would remain one of the equivalent valid representations of the target dynamics.

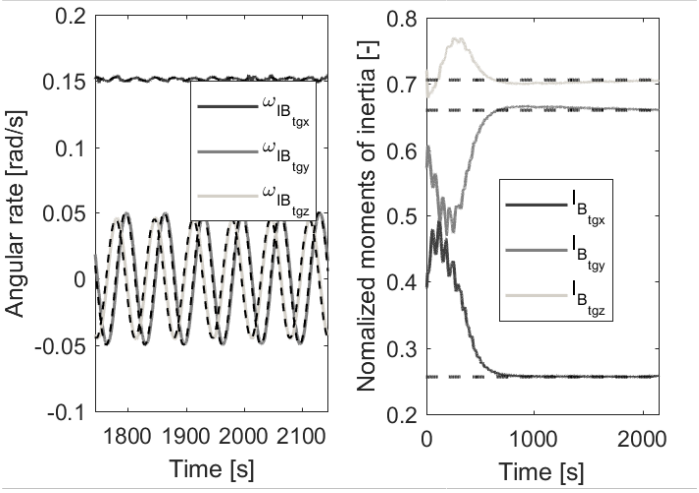

Fig. 6: estimated angular rate and inertia ratios. The estimation errors stabilize at about 700 seconds (simulation time)

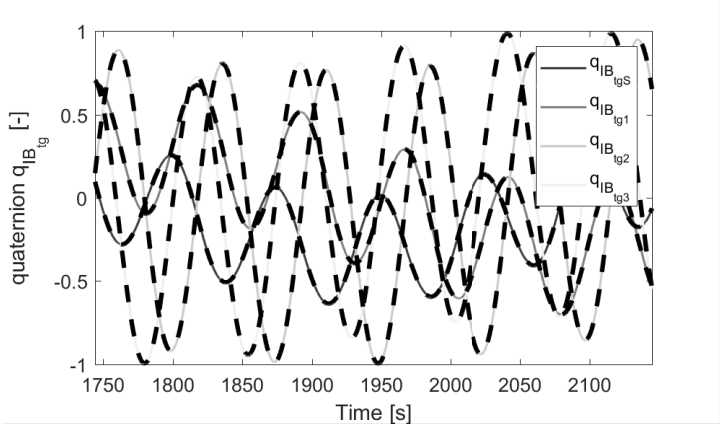

Fig. 7: estimated attitude quaternions $q_{IB_{tg}}$

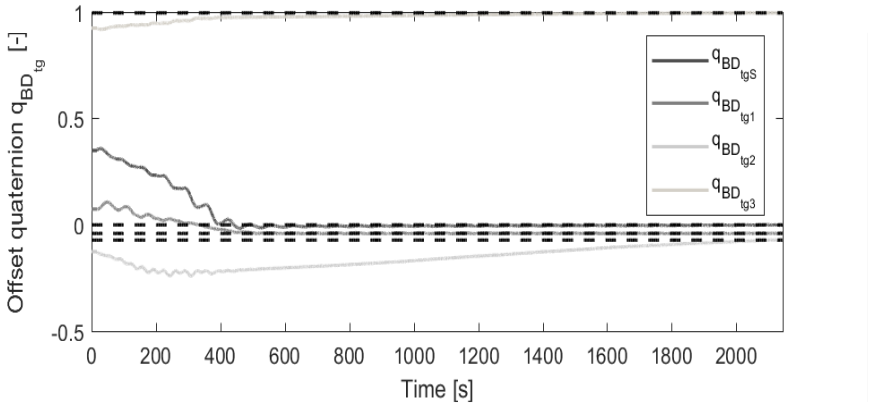

Fig. 8: estimated offset quaternions q_{DB}

The angular rate error behavior is shown in Fig.8. The errors have a non-random behavior, but the mean value of each error component is less than 10^{-5} rad/s. The three root mean square errors (RMSE) are respectively equal to $7 \cdot 10^{-4}$ rad/s, $5.5 \cdot 10^{-3}$ rad/s and $5.4 \cdot 10^{-3}$ rad/s. Maximum errors are in the order of 10^{-2} rad/s.

The errors in the estimation of the attitude quaternions $q_{IB_{tg}}$ are illustrated in Fig. 9. In this case, the errors seem to be more randomly distributed, but it is still possible to note low-frequency components. The mean values for the four components of the error are in the order of 10^{-4} rad, while the four RMSE for the quaternion components are all similar and in the order of $2 \cdot 10^{-3}$ rad.

To have a better illustration of the performances of the proposed estimation technique with simulated data, it is possible to see the work in [26], in which several application cases are discussed.

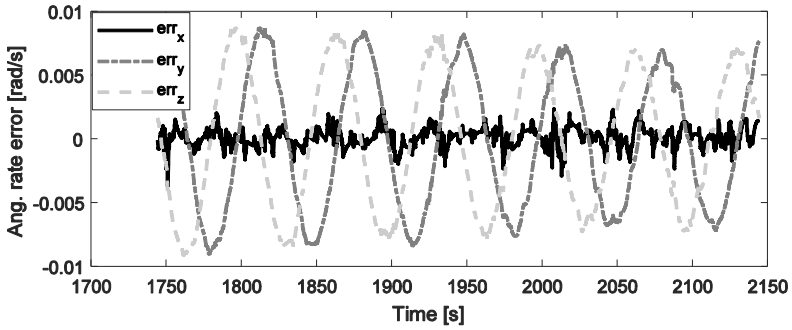

Fig. 9: errors in estimating angular rate

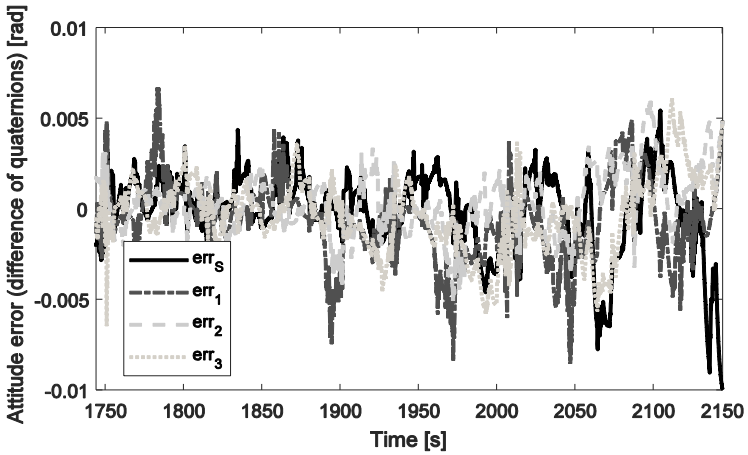

Fig. 10: errors in estimating attitude quaternions $q_{IB_{tg}}$

B. Experimental validation of the technique for the attitude recovery

The proposed method for attitude recovery via compressive sampling techniques was not tested only on simulated data but also in a laboratory environment. Clearly, the realization of a mock-up of the target that moves according to the laws of the celestial mechanics is an extremely difficult task, also in the case in which only the attitude dynamics should be reproduced. Indeed, there are not existent facilities that are capable of fully simulating the mentioned dynamics

The most famous laboratories that simulate the relative dynamics between satellites are more focused on the orbital dynamics. Typically, the test-bed comprises a flat-floor or a granite table facility in which frictionless motion is achieved by releasing compressed air from appropriate tanks within the mock-ups of the satellites. Two examples of this kind of laboratories can be found in [44] and [23]. There are also few other laboratories in which the mock-ups of the satellites are mounted on manipulators to better simulate the relative attitude dynamics. One example is in [45]: the air bearings for the two mock-ups support gimbals for allowing a 3 DOF attitude motion for the mock-ups. However, with that structure, the rotations of the mock-ups remain limited to few tens of degrees.

Politecnico di Torino does not own a specific facility for simulating spacecraft in formation flying. However, within the CADET program, Aviospace S.r.l. developed a test rig for the partial simulation of the relative motion between target and chaser satellites during a removal mission. The developed laboratory environment was called CADETLab [30]. This test-bed comprises a cylindrical-shaped target mock-up mounted on a mechanical architecture, which allows two rotational degrees of freedom and a translational one. The two rotational degrees of freedom consists of a rotation about the axis of symmetry of the mock-up (spinning motion), and of a rotation about a fixed axis that is parallel to the floor (tumbling motion). Clearly, with this architecture, the resulting attitude dynamics cannot be comparable to the one of a real satellite. The laboratory comprises also a monocular infrared (IR) camera for the target observation. A photo of the laboratory is shown in Fig.11

The algorithms presented in this work were tested in this laboratory. A third company, whose name is Blue Engineering s.r.l, was responsible for the CADET research program of a first coarse pose estimation of the target employing the mentioned IR.

Relying on the expectable consistent difference between the temperature of the target and the environment, Blue engineering exploited several known filtering algorithms to identify approximately the contour of the target. In the CADETLab environment, the target mock-up was appropriately heated by the usage of high-power lamps.

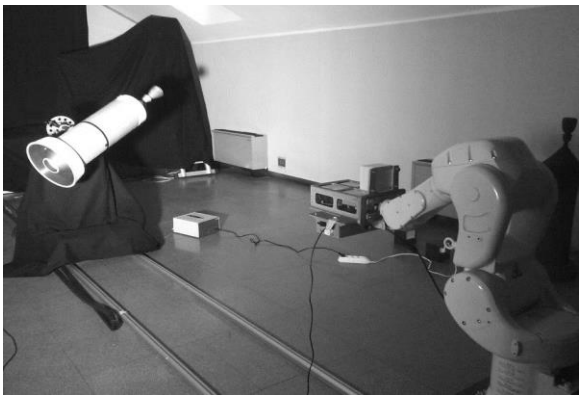

Fig. 11: The CADETLab Environment. The IR camera is mounted on an articulated robotic arm

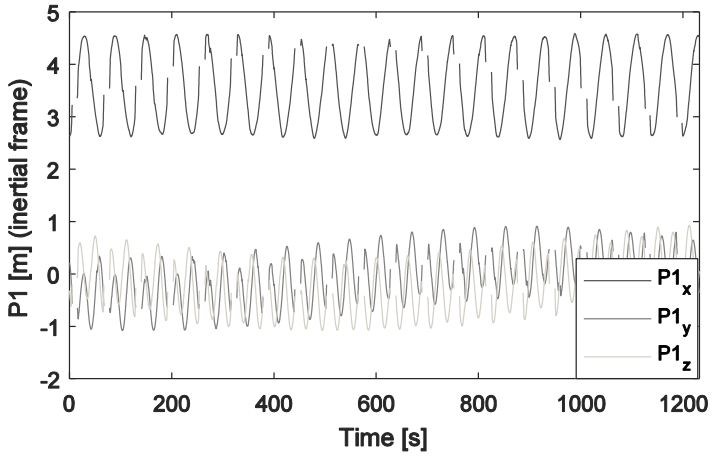

Fig. 12: Coordinates of the point *P*1 after the elaboration of IR images by Blue Engineering during a test

From the possession of a CAD model of the mock-up, which is equivalent to assuming the knowledge of prior information about the target shape, they performed a 3D rendering of the found contour. Thus, they attached three points to this rendered model evaluating their position for each time sample.

The data relative to one of those three points ($P1$, $P2$, $P3$) taken during a test are shown in Fig. 12. Note from the latter figure that several missing samples are present due to failures of the image elaboration process. During this test the target mock-up was moved imposing two constant angular velocities: 0.96 rpm for both the two degrees of

freedom. Note that the stepper motors used to move the target were open-loop controlled, so the nominal values of those velocities cannot be considered perfectly reliable.

Equation (1) is used to evaluate surrogate quaternion measurements q_{DI} to which apply the presented technique for recovering attitude. Because of the inconsistency of the time evolution of the recovered attitude with the process in (10), the recovered $\tilde{q}_{ID}$ was used to feed a Kalman filter with a simple triple integrator model:

$$x_{k+1} = \begin{bmatrix} \tilde{q}_{ID} \\ \dot{\tilde{q}}_{ID} \\ \ddot{\tilde{q}}_{ID} \end{bmatrix}_{k+1} \quad ; \quad x_{k+1} = \begin{bmatrix} \mathbf{1} & t\mathbf{1} & \frac{t^2}{2}\mathbf{1} \\ \mathbf{0} & \mathbf{1} & t\mathbf{1} \\ \mathbf{0} & \mathbf{0} & \mathbf{1} \end{bmatrix} x_k + w_k \tag{31}$$

where $\mathbf{1}$ is an identity matrix of proper dimension and $\mathbf{0}$ is an appropriate null matrix. The inertia ratios are not observable due to the mentioned inconsistency. The angular rate ω_{ID} is obtained through:

$$\omega_{ID} = 2\left(\tilde{q}_{ID_S}\dot{\tilde{q}}_{ID_V} - \tilde{q}_{ID_V}\dot{\tilde{q}}_{ID_S}\right) - 2\,\tilde{q}_{ID_V} \times \dot{\tilde{q}}_{ID_V} \tag{32}$$

where $\tilde{q}_{ID_V}$ is the vectorial part of the quaternion $\tilde{q}_{ID}$. The estimated ω_{ID} is the unique quantity that can be compared with the reference values of the angular speed imposed to the two stepper motors that guide the mock-up. Figure 13 illustrates the result of the estimation after the attitude recovery. Figure 14 and Fig. 15 provide the same estimated angular rate split into the two components according to the two motion primitives of the mock-up.

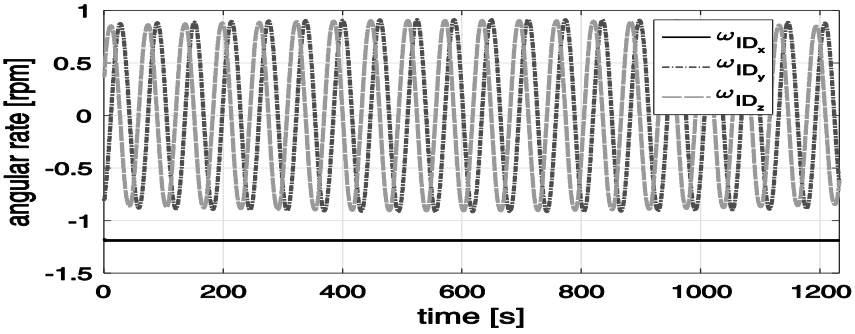

Fig. 13: Estimated angular rate of the target mock-up during a test

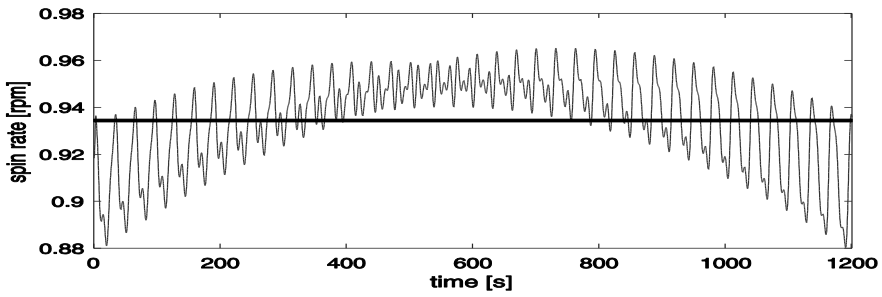

Fig. 14: Estimated spinning rate of the target mock-up during a test

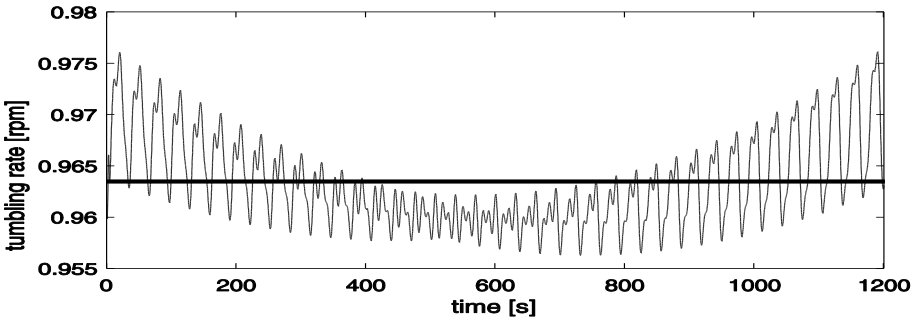

Fig. 15: Estimated tumbling rate (rotation axis parallel to the floor) of the target mock-up during a test

The two components were obtained by knowing that the constant angle formed by the two rotation axes was 76 deg. The mean value of the estimated spin rate is equal to 0.934 rpm, so a bias of 0.026 rpm, equal to $2.7 \cdot 10^{-3}$ rad/s, exists with respect to the nominal value of 0.96 rpm. The difference between the maximum and the minimum deviations over all the observation time is equal to 0.09 rpm, that is $9.4 \cdot 10^{-3}$ rad/s.

The mean value of the estimated tumbling rate is equal to 0.965 rpm while the nominal value was 0.96 rpm. Thus, bias is negligible in this case. The difference between the maximum and the minimum deviations from the mean value is equal to 0.021 rpm, whose corresponding value in rad/s is $2.2 \cdot 10^{-3}$. Those results are quite encouraging and are completely in line with the results obtained from simulated data.

C. Catching maneuver

The second and third phases on the mission profile consist of the execution of the fly around and the straight line maneuvers, respectively. Once the angular velocity of the target has been estimated, it is possible to determine the rotation axis, considered as mating axis. Starting from the normalized values of the estimated angular velocity (ω_{norm}^{ib})

of target-wrt inertial frame the corresponding value in orbital frame is evaluated via the rotation matrix, characterized by the orbital parameters as:

$$\omega_{TOL}^{T} = L_{bTOL}\omega_{ib}^{T}$$

The desired attitude for the whole duration of the final approach is the target pointing mode as showed in Fig. 16

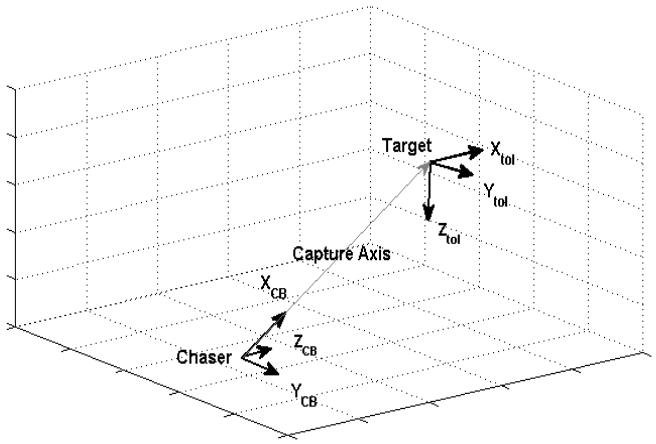

Fig. 16: Example of chaser pointing attitude

A simple algorithm is used to compute the director cosines matrix R_{TP} (subscript TP indicates target-pointing frame) of the reference chaser attitude based on its rotation axis as:

$$R_{TP} = [a_1 \quad a_2 \quad a_3] = \quad \rightarrow \quad \begin{cases} \vec{a}_1 = -ca_0 \\ \vec{a}_3 = ca_0 \wedge \vec{Y}_{TOL} \\ \vec{a}_2 = \vec{a}_3 \wedge \vec{a}_1 \end{cases}$$

where:

- ca_0 is the desired capture axis equal to the instantaneous rotation axis
- $\vec{Y}_{TOL} = [0 \quad 1 \quad 0]$ – Y-axis of the Target orbital local frame

The director vectors a_1,a_2 and a_3 form an orthonormal frame of reference with:

- X-axis oriented in the same direction of the relative position vector, toward the target.
- Y-axis oriented normal to X-axis and Y_{TOL}
- Z-axis which forms a right-handed orthonormal frame

The Chaser attitude will head towards the target orbital reference frame, in order to guarantee the correct attitude and approach to the target, with respect to the capture axis. This reference frame is evaluated with respect to the Y orbital local frame due to the unsafe manoeuvre related to a Z (R-bar) approach.

Fig. 17 reports a representation of the tumbling axis approach manoeuvre:

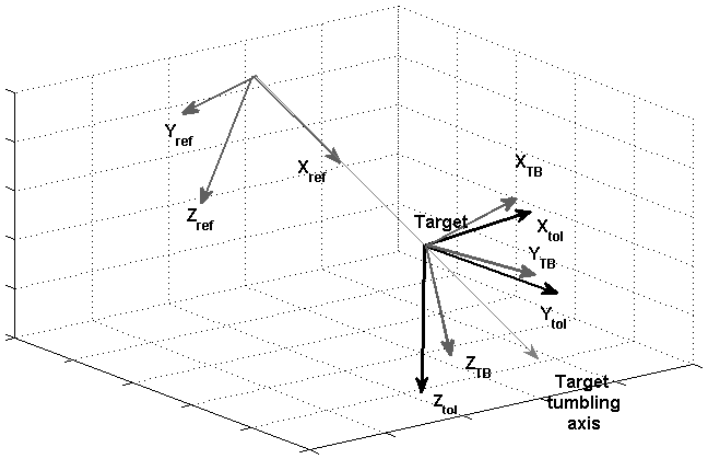

Fig. 17: Tumbling axis approach manoeuver

Concerning the motion of the capture axis related to the target body, which describe a cone following the periodic motion of the angular momentum vector as shown in Fig. 18, it is possible to estimate the position of the rotation axis at the end of the rendezvous maneuver.

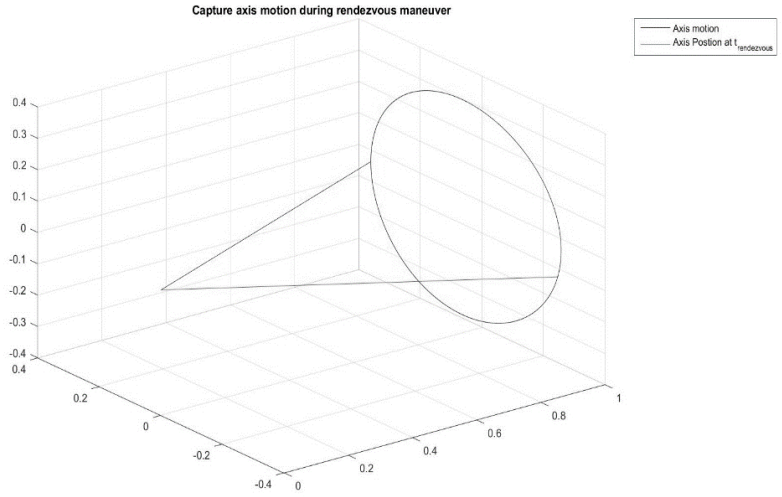

Fig. 18: Tumbling axis motion in target orbital reference frame

This approximation takes into account margin for the uncertainties related to the estimation process, indeed, thanks to the chosen approach it is possible to compensate those during the close approach maneuver.

Normalizing the estimated angular velocity, in orbital reference frame, the estimated mating axis at the end of the rendezvous maneuver is defined as [-0.95022, 0.2986, 0.0885]. In this way, it is possible to define the line that has origin in O_{CH} and inclination 17.37°, -5.32° and 0.1° with respect to, respectively, x-axis, y-axis and z-axis of the Chaser Local Orbital Frame, that are the desired values for the attitude controller.

Fig. 19 shows the trend in time of the three components of the relative position between Chaser and Target in the Target orbital frame. The two phases of maneuver are highlighted: the fly-around maneuver lasts about 245, until the tumbling axis is intercepted in the point [-28.88, 8.73, 2.61] m with respect to the Target Local Orbital frame. In the second phase, the straight line maneuver along the tumbling axis is performed in about 325 seconds. The complete maneuver lasts about 570 seconds.

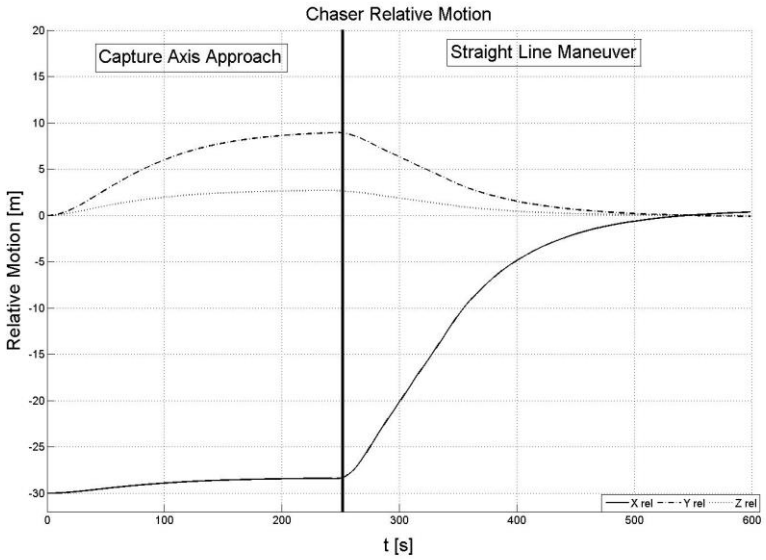

Fig. 19: Relative position between Chaser and Target Local Orbital frame

Fig. 20 shows the highlights of the velocity trends in the two phases: the docking point is reached with a lateral velocity of 0.008 m/s and an approach 0.009 m/s a.

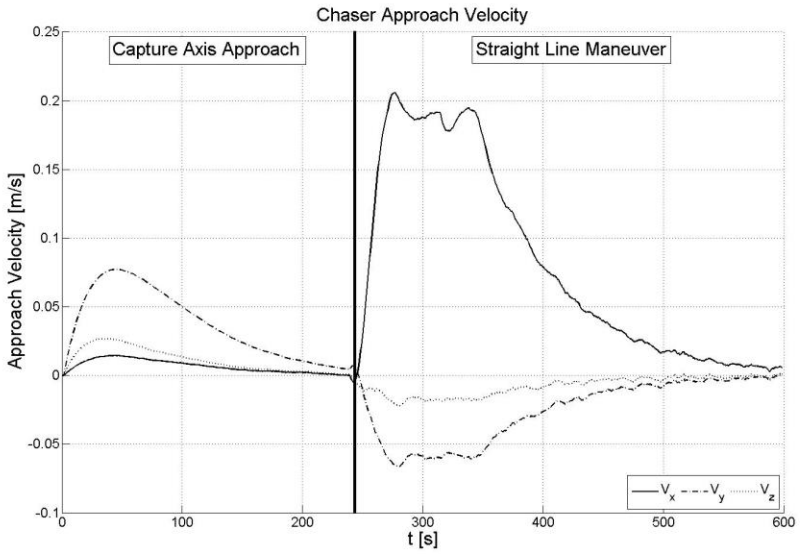

Fig. 20: Highlights of the relative velocity in the two phases of maneuver

Fig. 21 shows the trend in time of the Chaser attitude, expressed as Euler angles, on the left. In particular dotted lines indicate the desired attitude and the full lines represent the actual attitude value. In particular, the figure shows the details of the attitude during the fly-around maneuver (on the left) and the straight-line approach (on the right), underlining the capability of the controller to track the reference value. At the mating point, the angular misalignment is less than 0.01 deg with respect to the desired attitude for any axis.

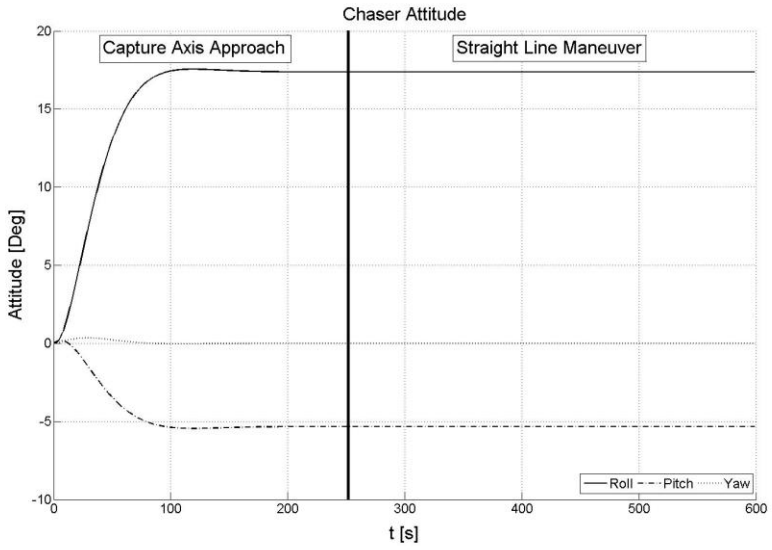

Fig. 21: Attitude highlights in the two phases of maneuver

The Chaser angular velocity for the two phases of maneuver is shown in Fig. 22. During both the phases the angular velocity is very low with a peak of less than 0.3 deg/s and, at the mating point, the angular velocity is less than 0.01 rad/s.

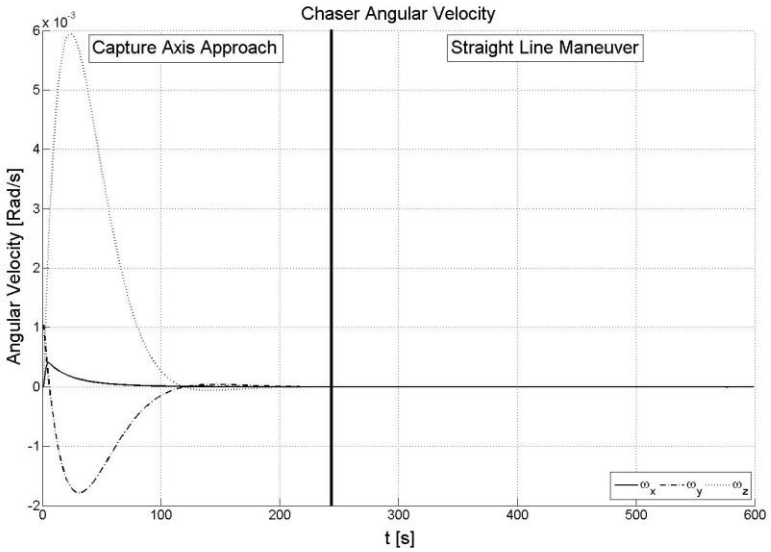

Fig. 22: Chaser angular velocity for the two phases of maneuver

Table 4 summarizes the final values of the parameters at the docking point. It is noticed that all the performances required for a soft-docking approach have been reached.

	Final Value at mating point	Required Performance
Approach velocity [m/s]	0.008	<0.03
Lateral alignment [m]	0.032	<0.20
Lateral velocity [m/s]	0.011	<0.05
Angular misalignment [deg]	0.01	<1
Angular rate [deg/s]	0.009	<0.05

Table 4: comparison between required and obtained requirements

VI. Conclusion

The paper deals with the final approach and mating for spacecraft close proximity operations in missions of active debris removal providing new solutions both for the on orbit estimation of the target motion and for the final maneuvers strategies. The target motion and physical properties are estimated through the analysis of images taken from the final hold point: the target inertial matrix and angular velocities derive from the analysis of particular features

individuated on the pictures handled thanks to the application of the innovative algorithms proposed in this paper. The knowledge of the target motion allows the definition with good confidence of the rotation axis of the target with respect to the target body frame. The rotation axis becomes the mating axis in the guidance strategies it means that final approach can be performed along a wider range of axes with respect to the well-known and traditional axes (mainly, V-bar and R-bar). The proposed controller can drive the chaser spacecraft to the desired position and attitude precisely in approach of space target. It takes into account crucial aspects such as the trajectory tracking control and the input constraint control.

The obtained results are very promising and encourage a future deeper investigation. Future works should focus on reducing the assumptions needed for an accurate estimation of the target attitude: the current algorithm needs the knowledge of the relative positions of the tracked features in a neutral reference frame, such as a CAD model of the target. From the guidance point of view, future activities should be addressed to extend the range of possible guidance approaches (for example, considering the fly-around maneuvers) in order to cover the widest possible range of final approach maneuver. For the control aspects, future works should be based on complicating the problem by extending the strategies in this work, considering finite-time control and more stringent input constraints as well as enrich the presented model with other uncertainties parameters.

Acknowledgments

This work has been developed within the CADET research program. CADET project is co-ordinated by Aviospace srl - an EADS Astrium company; it is co-funded by Regione Piemonte in the frame of programme: POR FESR 2007/2013 - linea di attività I.1.1. ``Piattaforme innovative" - AEROSPAZIO FASE II. .

References

[1] Cooney M., “NASA identifies Top Ten space junk missions”, *Network World*, 28 July 2010

[2] Kessler D.J., Johnson N.L., Liou J.C., Matney M., “The Kessler Syndrome: Implications to Future Space Operations”, *33rd Annual AAS Guidance and Control Conference*, Breckenridge, Colorado 2010

[3] Liou J.C., Hall D.T., Krisko P.H., Opiela J.N., “LEGEND, a 3-dimensional LEO to GEO Debris Evolutionary Model”, *Advances in Space Research*, Vol 34, No 5, 2004, Pages 981–986, doi:10.1016/j.asr.2003.02.027

[4] Liou J.C., Johnson N.L., Hill N.M., “Controlling the Growth of Future LEO Debris Population with Active Debris Removal”, *Acta Astronautica*, Vol. 66, No 5–6, March–April 2010, Pages 648–653, doi:10.1016/j.actaastro.2009.08.005

[5] Richard M., Kronig l., Belloni F., Rossi S., Gass V., Paccolat C., Thiran J.P., Araomi S., Gavrilovich I., Shea H., "Uncooperative Rendezvous and Docking for MicroSats1 .The case for CleanSpace One", *6th International Conference on Recent Advances in Space Technologies*, RAST 2013, 12-14 June 2013, Istanbul, Türkey

[6] Forshaw J.L., et al., "An In-Orbit Active Debris Removal Mission – Remove DEBRIS: Pre-launch Update", *Proceedings of the 66th International Astronautical Congress (IAC 2015)*, Jerusalem, Israel, Oct.12-16, 2015

[7] Wormnes, R. et al., "ESA Technologies for Space remediation", *6th European Conference on Space Debris, Proceedings of the conference*, 22-25 April 2013, Darmstadt, Germany, ISBN 978-92-9221-287-2, 2013, id.

[8] Sommer J., Ahrns I., "GNC for a Rendezvous in Space with an Uncooperative Target." *5th International Conference on Spacecraft Formation Flying Missions and Technologies*, Munich (Germany), May 2013.

[9] Wertz J.R., Bell R., "Autonomous rendezvous and docking technologies—Status and prospects," in *Proc. Int. Soc. Opt. Eng*., vol. 5088, pp. 20–30, Apr. 2003. doi:10.1117/12.498121

[10] Cresto Aleina S., Viola N., Stesina F., Viscio M.A., Ferraris S., Reusable space tug concept and mission, Acta Astronautica, vol. 128, pag 21-32, 2016, doi: 10.1016/j.actaastro.2016.07.003

[11] Di Cairano , S. Park , H. Kolmanovsky, "Model Predictive Control Approach for Guidance of Spacecraft Rendezvous and Proximity Maneuvering", in Int. Journal of Robust and Non Linear Control, vol 22, 30 pages, 2012, doi: 10.1002/rnc.2827

[12] Arantes G., Martins-Filho L.S., "Guidance and Control of Position and Attitude for Rendezvous and Dock/Berthing with a Non cooperative/Target Spacecraft", *Mathematical Problems in Engineering*, Vol. 2014, Article ID 508516, 8 pages, doi:10.1155/2014/508516

[13] Arantes Jr. G., Komanduri A., Martins Filho L. S., "Guidance for rendezvous maneuvers involving non-cooperative spacecraft using a fly-by method," in *Proceedings of 21st International Congress of Mechanical Engineering (COBEM '11)*, Natal,Brazil, October 2011.

[14] Machula M. F., Sandhoo G. S, "Rendezvous and docking for space exploration", *Proceedings of 1st Space Explorat. Conf.: Contin. Voyage Discov*., Orlando, FL, Jan. 2005, doi: 10.2514/6.2005-2716

[15] Aghili F., "A Prediction and Motion-Planning Scheme for Visually Guided Robotic Capturing of Free-Floating Tumbling Objects With Uncertain Dynamics", *IEEE TRANSACTIONS ON ROBOTICS*, VOL. 28, No. 3, JUNE 2012. doi: 10.1109/TRO.2011.2179581

[16] Matsumoto S.et al. "Satellite capturing strategy using agile orbital servicing vehicle, hyper OSV," *Proc. IEEE Int. Conf. Robot. Autom*., Washington, DC, May. 2002, pp. 2309–2314, doi: 10.1109/ROBOT.2002.1013576

[17] Lichter M.D., Dubowsky S., "State, shape, and parameter estimation of space objects from range images." *Robotics and Automation, 2004. Proceedings. ICRA'04. 2004 IEEE International Conference on*. Vol. 3. IEEE, 2004, doi: 10.1109/ROBOT.2004.1307513

[18] Aghili, F., et al. "Fault-tolerant position/attitude estimation of free-floating space objects using a laser range sensor." *Sensors Journal, IEEE* 11.1 (2011): 176-185. doi: 10.1109/JSEN.2010.2056365

[19] Iqbal, J. et al. "Real-time Target detection and tracking: A comparative in-depth review of strategies." *Life Science Journal* 10.3 (2013): 804-813

[20] Lim Seong-Min, Hae-Dong Kim, Jae-Dong Seong. "Vision-based Ground Test for Active Debris Removal." *Journal of Astronomy and Space Sciences* 30.4 (2013): 279-290, doi: 10.5140/JASS.2013.30.4.279

[21] Li, N., et al. "Tracking the Trajectory of Space Debris in Close Proximity via a Vision-Based Method." *Journal of Aerospace Engineering* 27.2 (2014): 238-248. doi: 10.1109/ACC.2011.5991383

[22] Terui F., Heihachiro K., Shinichiro N. "Motion estimation to a failed satellite on orbit using stereo vision and 3D model matching." *Control, Automation, Robotics and Vision, 2006. ICARCV'06. 9th International Conference on*. IEEE, 2006, doi: 10.1109/ICARCV.2006.345305

[23] Segal S., Avishy C., Pini G., "Stereovision-based estimation of relative dynamics between non cooperative satellites: theory and experiments." *Control Systems Technology, IEEE Transactions on* 22.2 (2014): 568-584, doi: 10.1109/TCST.2013.2255288

[24] Oumer N.W., Panin G., "3D point tracking and pose estimation of a space object using stereo images", *2012 21st International Conference on Pattern Recognition (ICPR)*. IEEE, 2012.

[25] Biondi G., Mauro S., Mohtar T., Pastorelli S., Sorli M., "A geometric method for estimating space debris center of mass position and orbital parameters from features tracking." *Metrology for Aerospace (MetroAeroSpace)*. IEEE, 2015. doi: 10.1109/MetroAeroSpace.2015.7180666

[26] Biondi G., et al. "Attitude recovery from feature tracking for estimating angular rate of non-cooperative spacecraft." *Mechanical Systems and Signal Processing* 83 (2017): 321-336., doi: 10.1016/j.ymssp.2016.06.017

[27] Corpino S., Stesina F., "Verification of a CubeSat via Hardware-in-the-loop Simulation". *IEEE Transaction on Aerospace and Electronic Systems*, vol. 50, ISSN: 0018-9251,2014, doi: 10.1109/TAES.2014.130370

[28] Fhese J., *Automated Rendezvous and Docking of Spacecraft*, Cambridge University Press, 2003, ISBN 0 521 82492 3

[29] http://www.braeunig.us/space/specs/ariane.htm. Last access 11 November 2016

[30] Chiesa A., Fossati F., Gambacciani G., Pensavalle E., "Enabling Technologies for Active Space Debris Removal: The Cadet Project,", in *"Space Safety is No Accident"*, pp.29-38, January 2015, doi: 10.1007/978-3-319-15982-9_4

[31] Schaub, Hanspeter. *Analytical mechanics of space systems*. AIAA, 2003, pp 85-91

[32] Candès, J. "Compressive sampling." *Proceedings of the international congress of mathematicians*. Vol. 3. 2006.

[33] Tropp J., "Just relax: Convex programming methods for identifying sparse signals in noise." IEEE Transactions on Information Theory, 52.3 (2006): 1030-1051. doi: 10.1109/TIT.2005.864420

[34] Manya A., Bioucas-Dias J.M., Figueiredo M. "Fast image recovery using variable splitting and constrained optimization.", *IEEE Transactions on Image Processing,* 19.9 (2010): 2345-2356. doi: 10.1109/TIP.2010.2047910

[35] Carmi, A., Gurfil P., Kanevsky D. "Methods for sparse signal recovery using Kalman filtering with embedded pseudo-measurement norms and quasi-norms." *IEEE Transactions on Signal Processing* 58.4 (2010): 2405-2409. doi: 10.1109/TSP.2009.2038959[36] Julier S., Uhlmann J.K. "Unscented filtering and nonlinear estimation." *Proceedings of the IEEE* 92.3 (2004): 401-422, doi: 10.1109/JPROC.2003.823141

[37] Gaias, G., D'Amico S., J-S. Ardaens. "Angles-only navigation to a noncooperative satellite using relative orbital elements." *Journal of Guidance, Control, and Dynamics* 37.2 (2014): 439-451. doi: 10.2514/1.61494

[38] Van Der Merwe R., Wan E., "The square-root unscented Kalman filter for state and parameter-estimation." *Acoustics, Speech, and Signal Processing, 2001. Proceedings.(ICASSP'01). 2001 IEEE International Conference on*. Vol. 6. IEEE, 2001, doi: 10.1109/ICASSP.2001.940586

[39] Sabatini, Angelo Maria. "Kalman-filter-based orientation determination using inertial/magnetic sensors: Observability analysis and performance evaluation." *Sensors* 11.10 (2011): 9182-9206, doi: 10.3390/s111009182

[40] Crassidis, John L., and F. Landis Markley. "Unscented filtering for spacecraft attitude estimation." *Journal of guidance, control, and dynamics* 26.4 (2003): 536-542, doi: 10.2514/2.5102

[41] Psiaki, Mark L. "Estimation of a spacecraft's attitude dynamics parameters by using flight data." Journal of Guidance, Control, and Dynamics 28.4 (2005): 594-603, doi: 10.2514/1.7362

[42] Foley J et al., *Introduction to computer graphics*, Vol.55. Reading: Addison-Wesley, 1994, pp. 1023-1065

[43] Brack, D N., Gurfil P. "In-Orbit Tracking of High Area-to-Mass Ratio Space Objects." *Journal of Guidance, Control, and Dynamics* (2017). doi: 10.2514/1.G002501

[44] Bevilacqua R., Lehmann T., Romano M. "Development and experimentation of LQR/APF guidance and control for autonomous proximity maneuvers of multiple spacecraft." *Acta Astronautica* 68.7 (2011): 1260-1275. doi: 10.1016/j.actaastro.2010.08.012

[45] Valmorbida A. et al. "Attitude module characterization of the satellite formation flight testbed." Metrology for Aerospace (MetroAeroSpace), 2014 IEEE. IEEE, 2014. doi; 10.1109/MetroAeroSpace.2014.6865897